HHS Public Access

Author manuscript

Neuroimage. Author manuscript; available in PMC 2019 March 01.

Published in final edited form as:

Neuroimage. 2018 March ; 168: 412–426. doi:10.1016/j.neuroimage.2017.02.052.

Challenges and opportunities for brainstem neuroimaging with ultrahigh field MRI

Roberta Sclocco[1,2], **Florian Beissner**[3], **Marta Bianciardi**[1], **Jonathan R. Polimeni**[1,4], and **Vitaly Napadow**[1,2]

[1]Athinoula A. Martinos Center for Biomedical Imaging, Massachusetts General Hospital, Harvard Medical School, Boston, MA, USA

[2]Department of Radiology, Logan University, Chesterfield MO, USA

[3]Somatosensory and Autonomic Therapy Research, Institute for Neuroradiology, Hannover Medical School, Hannover, Germany

[4]Harvard-MIT Division of Health Sciences and Technology, Massachusetts Institute of Technology, Cambridge, MA, USA

Abstract

The human brainstem plays a central role in connecting the cerebrum, the cerebellum and the spinal cord to one another, hosting relay nuclei for afferent and efferent signaling, and providing source nuclei for several neuromodulatory systems that impact central nervous system function. While the investigation of the brainstem with functional or structural magnetic resonance imaging has been hampered for years due to this brain structure's physiological and anatomical characteristics, the field has seen significant advances in recent years thanks to the broader adoption of ultrahigh-field (UHF) MRI scanning. In the present review, we focus on the advantages offered by UHF in the context of brainstem imaging, as well as the challenges posed by the investigation of this complex brain structure in terms of data acquisition and analysis. We also illustrate how UHF MRI can shed new light on the neuroanatomy and neurophysiology underlying different brainstem-based circuitries, such as the central autonomic network and neurotransmitter/neuromodulator systems, discuss existing and foreseeable clinical applications to better understand diseases such as chronic pain and Parkinson's disease, and explore promising future directions for further improvements in brainstem imaging using UHF MRI techniques.

Keywords

medulla; pons; midbrain; mesencephalon; nociception

Correspondence to: Roberta Sclocco, PhD, Athinoula A. Martinos Center for Biomedical Imaging, CNY 149-2301, 13th St. Charlestown, MA 02129, roberta@nmr.mgh.harvard.edu.

1. Introduction

The human brainstem is one of the most challenging brain regions to study with either functional or structural magnetic resonance imaging (MRI). Its propensity to physiological (i.e. cardiorespiratory) noise as well as the small size and complexity of its anatomical constituents are brainstem-specific challenges that place high demands on image acquisition as well as data analysis methods. Nevertheless, the field of brainstem f/MRI has significantly advanced in recent years, partly due to the broader adoption of ultrahigh-field (UHF) MRI scanners (7 tesla and higher), as well as several methodological advances that facilitate brainstem neuroimaging. In this context, our review focuses on these technical advances at UHF as well as the neuroscience underlying different brainstem-based circuitries and neurotransmitter systems and their clinical applications. Importantly, while UHF provides several advantages for brainstem imaging, there are also limitations, and some excellent research at lower fields (e.g. 3T) has indeed improved our understanding of brainstem structure and function, and is also reviewed here.

Much of the brainstem's important role can be inferred by its anatomical location. It is a central structure that connects the cerebrum and cerebellum to each other and to the spinal cord. Virtually all afferent and efferent signaling involving peripheral receptors and effectors (e.g. muscles, glands) relays with brainstem nuclei on their way to or from the spinal cord or cranial nerves III-XII. Important processing occurs in these relay nuclei, and the brainstem, as one of the phylogenetically oldest structures of the brain (Mai et al. 2004), is a key region for almost all primitive survival-oriented (e.g., fight or flight responses) functional and neuromodulatory systems. More specifically, brainstem nuclei synthesize and release specific neurotransmitters and neuromodulators for the regulation of such basic functions as arousal, motor function, memory, reward, nociception, and autonomic control.

Anatomically, the brainstem can be divided along its rostro-caudal axis into midbrain (or mesencephalon), pons, and medulla oblongata (see Figure 1). The midbrain adjoins the diencephalon (consisting primarily of thalamus and hypothalamus), which constitutes the upper border of the brainstem, whereas the medulla oblongata merges into the spinal cord. Along a dorsoventral axis, the brainstem consists of the tectum, which includes structures dorsal to the mid-point of the cerebral aqueduct, the tegmentum, a central region of neurons and fibers containing the so called reticular formation and several other nuclei, and a ventral white matter fiber communication system connecting the cerebral cortex to the spinal cord and the cerebellum.

2. The potential of UHF MRI to overcome brainstem-specific imaging challenges

Despite the major role of the human brainstem in systems and circuitries that are otherwise extensively studied in neuroscience, it has received little attention from the neuroimaging community relative to studies of the cortex or even subcortical structures (e.g. striatum, thalamus). This is mainly due to several challenges specific to the brainstem. In the following section we will explore these challenges in detail and demonstrate how UHF MRI may help to overcome them.

2.1 Small cross-sectional area of brainstem nuclei and tracts

MRI studies estimated that the average brainstem volume in healthy adults is about 34 ml (Luft et al. 1999), and the average diameters of its subdivisions range from 18 mm in the midbrain, to 30 mm in the pons, to 14 mm in the medulla (Raininko et al. 1994). Brainstem nuclei, which are commonly elongated along the craniocaudal brainstem axis, have an average cross-sectional diameter of only a few millimeters (Afshar et al. 1978). They are, thus, considerably smaller than the cortical and diencephalic structures more commonly imaged with MRI (see Table 1). The same holds true for brainstem white matter fiber tracts, although to a lesser extent. The small cross-sectional area of brainstem anatomical constituents is a major challenge for imaging. This is particularly true when using fMRI at field strengths of 3 tesla and below, where achieving an adequate signal-to-noise ratio for voxels near the center of the head requires an in-plane spatial resolution in the order of 2-4 mm. Consequently, imaging brainstem physiology with fMRI at 3 tesla means working at the spatial resolution limit (Beissner 2015).

Two of the main advantages offered by structural and functional UHF imaging are the increased signal-to-noise ratio (SNR) and, in some cases, further increases in contrast-to-noise ratio (CNR). Their combined effects allow for the reduction of voxel size relative to 3 tesla MRI with no significant signal loss, opening the door to sub-millimeter spatial resolution, and revealing detailed anatomical information invisible at lower field strengths (Cho et al. 2014). Several structural and functional studies have exploited this opportunity to image brainstem nuclei and tracts at unprecedented spatial resolution (Bianciardi et al. 2015; Blazejewska et al. 2013; Cho et al. 2014; Deistung et al. 2013; Faull et al. 2015; Prats-Galino et al. 2012; Satpute et al. 2013; Sclocco et al. 2016; Wargo and Gore 2013).

A major benefit of fMRI at ultra-high fields is the supralinear increase of the change of the effective transverse relaxation rate (ΔR_2^*) of brain tissue with the change in concentration of deoxygenated blood that translates to a larger change in the blood oxygenation level-dependent (BOLD) signal. Importantly, this increase occurs only for the extravascular signal contribution near small vessels such as capillaries, while the increase near large draining vessels is linear (Boxerman et al. 1995), leading to both improved spatial resolution and spatial specificity for UHF fMRI. A crucial consequence of this effect for fMRI studies is a general increase in statistical power, allowing for a reduction of the number of subjects required for multi-subject averaging compared to lower field strengths (Chang et al. 2016). While this is mostly true for cortical areas, when investigating structures with a small cross-sectional area (e.g. brainstem nuclei), the variability across subjects plays a major role and could potentially override the benefit of UHF. Additionally, this issue is aggravated by the lack of a probabilistic brainstem atlas, which can map the location of different nuclei in a standard space (see Section 6 for more detail). Finally, the necessity to morph individual images into a standard space using algorithms and atlases mainly designed for cortical structures might further contribute to decrease the specificity offered by UHF.

In terms of fMRI data acquisition, a viable target for maximum voxel size would be 2 mm isotropic in-plane resolution, though at UHF, significantly smaller voxel sizes, in the order of 1 mm isotropic in-plane, are preferable depending on experiment design. In terms of data analysis, spatial smoothing kernels for fMRI data should be carefully considered. On the one

hand, standard filtering theory suggests that the “best” smoothing filter or kernel is one that matches the feature size, therefore smoothing kernels should be in the order of expected activation extent. On the other hand, there is a constraint on the lower limit of smoothing given by Gaussian field theory, which requires a voxel size appreciably smaller than the spatial smoothness. Therefore, smoothing kernels have been recommended to be at least twice the voxel size (Worsley and Friston 1995). From a practical standpoint, slightly larger kernels may be necessary for brainstem imaging due to inter-subject variability in the exact nucleus location once individual data have been registered onto standard space templates. While such variability is unknown for many nuclei, a recent study of locus coeruleus imaging in the pons found that this nucleus can shift in position by at least 2-3 mm in MNI space localization within the axial plane of the brainstem (Keren et al. 2009). Other recommendations for analysis also include preprocessing with brainstem masked analyses to (1) limit physiological noise artifacts from surface vessels (i.e. important to mask prior to spatial smoothing, see below), and (2) reduce the multiple comparisons correction problem by reducing the number of voxels in the analysis (relative to whole brain scanning).

Due to the small cross-sectional area of most brainstem nuclei, correction for multiple comparisons should utilize voxel-based correction approaches, as opposed to cluster-based approaches that are skewed to larger activation clusters. Furthermore, nonparametric approaches (e.g. permutation testing) or Bayesian statistics, are preferred to parametric general linear models, as smoothness assumptions associated with the latter are often not met in the brainstem (Beissner et al. 2011). For example, the use of Gaussian field theory to threshold activations assumes a smoothness of at least twice the voxel size. For lower values, the corrected p-values derived from Gaussian random fields will approach those of Bonferroni correction, which is overly conservative, leading to potentially false negative results (Worsley and Friston 1995). Nonparametric methods usually do not rely on smoothness assumptions, whereas Bayesian statistics handles smoothness as a spatial prior, rather than smoothing the data during pre-processing using fixed-width Gaussian kernels (Penny et al. 2005). Furthermore, as compared to standard approaches based on spatially smoothing the imaging data itself, a Bayesian spatial regularization procedure has been shown to result in inferences with higher sensitivity (Penny et al. 2005), and may be promising for brainstem imaging.

Finally, physiological noise correction using one of the methods proposed in the literature is a must for brainstem analyses, due to the significant contribution of cardiorespiratory artifact to the brainstem fMRI signal (see below). Particular care should also be devoted to spatial co-registration and normalization, which would critically benefit from the adoption of brainstem-specific templates or co-registration approaches (see below).

2.2 Weak contrast of gray and white matter

Successful brainstem imaging is also hampered by weak contrast between gray and white matter structures. While both cerebrum and cerebellum show clear gray/white matter separation on T1, T2, and T2*-weighted imaging, this distinction is significantly weakened in the brainstem. Instead, gray matter parenchyma and white matter tracts are often intermingled in complicated structures, like the reticular formation or the basilar pons. Thus,

while the complexity of brainstem white/gray matter interdigitation is well known, standard MR imaging at 1.5 and 3 tesla usually shows the brainstem as a mostly homogeneous structure, save for iron-rich nuclei, like the substantia nigra and red nuclei in the midbrain. Recent work showed progress in discriminating between different tissue classes in the brainstem at 3T (Lambert et al. 2013), yet identification of individual brainstem nuclei could not be achieved. In contrast, UHF MRI offers several advantages for scientists and clinicians that are interested in localizing brainstem nuclei (Figure 2). Many MR parameters are field strength-dependent (see e.g. (van der Zwaag et al. 2015) for a recent review). Of special interest for the imaging of the brainstem and cranial nerves is the increase in magnetic-field-susceptibility-induced variations with higher B_0. The first advantage of this property is an increased phase contrast, leading to higher contrast-to-noise ratio (CNR) in susceptibility-weighted imaging (SWI). The quantitative version of this technique, called quantitative susceptibility mapping (QSM), is a post-processing method that computes maps of tissue magnetic susceptibility from the phase signals of gradient recalled echo (GRE) data (Reichenbach 2012). QSM has been reported to provide information about tissue iron content (Bilgic et al. 2012), brain myelination (Li et al. 2012), and blood oxygenation (Haacke et al. 2010). The increased magnetic susceptibility due to increased iron concentration is particularly useful to depict brainstem structures containing higher iron concentrations compared to the surrounding tissue, primarily the substantia nigra and red nuclei, but also inferior olive, spinal trigeminal nucleus and reticulotegmental nucleus (Deistung et al. 2013; Aggarwal et al. 2016). Additionally, Bianciardi et al. have recently used diffusion fractional anisotropy at 7-tesla to estimate the putative localization of several human brainstem nuclei *in vivo* (Bianciardi et al. 2015).

2.3 Physiological noise

Structural and functional MRI of the brainstem is highly sensitive to physiological (i.e. cardiorespiratory) noise sources of signal instability. Direct sources of this MRI signal instability include magnetic field changes due to chest motion (off-resonance B_0 effects), as well as pulsatility effects due to propagation of cardiac and respiratory pulse pressure waves in adjacent arteries, cerebrospinal fluid (CSF) spaces, and parenchyma. While multiple cortical and subcortical structures can be equally affected by CSF or arterial pulsatility, nuclei in the brainstem tend to be smaller than higher structures, and many are close to the brainstem border, where pulsatile artifacts transmitted along arteries and CSF can add significant noise to voxels encompassing both parenchyma and CSF/arteries. Moreover, the caudal location of the brainstem leads to a closer proximity to noise sources such as the heart and lungs (Brooks et al. 2013). Physiological noise in fMRI acquisitions increases with the field strength (Kruger and Glover 2001; Triantafyllou et al. 2005). Nevertheless, its contribution relative to thermal noise is mitigated by decreasing the voxel size, up to a regime where high spatial resolution fMRI images are dominated by thermal (rather than physiological) noise (Bodurka et al. 2007).

Chest motion due to respiration produces off-resonance B_0 effects due to changes in the concentration and spatial distribution of oxygen in the chest (note that molecular oxygen is paramagnetic). These effects introduce artifacts in functional (blurring, signal drop-out) and structural (also ghosting) MR images and low spatial frequency modulation in phase images

(Figure 3), which confound the investigation of tissue susceptibility and relaxivity. These effects are present both in structural and functional imaging, and increase with field strength. Previous 7 tesla studies (Bianciardi et al. 2014) showed that chest motion effects constitute a major noise component in phase data (explaining about 65% of signal variance) and a smaller (about 5% of signal variance) but not insignificant component in magnitude gradient-echo echo-planar imaging (EPI) fMRI data. These effects decrease with the cube of the distance from the center of the lungs (Raj et al. 2000), implying that inferior regions of the brain, such as the brainstem, suffer from higher signal instability and artifacts related to chest motion than other brain regions (see also Figure 3). Chest motion effects can be partially compensated by retrospective physiological noise correction strategies, that either use physiological recordings (Glover et al. 2000; Brooks et al. 2013) or respiratory-related information extracted from the image phase (Bianciardi et al. 2014). These effects can also be effectively reduced by the use of prospective external shimming procedures (van Gelderen et al. 2007), that are able to comprehensively monitor the magnetic field changes related to chest motion and compensate for them by controlling the frequency synthesizer, gradient coils and second order shims. In the future, we foresee that brainstem imaging at high and ultrahigh magnetic field will highly benefit from the development of higher order prospective shimming procedures based on the use of higher-order shim arrays (Juchem et al. 2011), or integrated RF-shim arrays driven by dynamically-controllable DC current drivers (Stockmann et al. 2016; Truong et al. 2014). Indeed, a recently built 3 tesla 32-channel RF-shim array rivals the performance of 4^{th}-order spherical harmonic shims and substantially reduces geometric distortion in high resolution single-shot EPI images, at the same time preserving the performance of both systems (RF detection and shim field generation) (Stockmann et al. 2016).

Pulsatility effects in the CSF (e.g. within the cerebral aqueduct) and large vessels due to propagation of cardiac and respiratory pressure waves produce significant artifacts for brainstem imaging. These artifacts mainly affect brainstem nuclei that are in close proximity with CSF spaces or large vessels. Thus, the most strongly affected regions are those adjacent to the aqueduct (e.g. periaqueductal grey, dorsal raphe nucleus), the fourth ventricle (i.e. the dorsal pontine tegmentum), the circle of Willis (e.g. ventral tegmental area) and vertebral/basilar arteries (i.e. almost the entire ventral and ventrolateral medulla oblongata). These high-susceptibility regions are evident by applying independent component analyses with unmasked brainstem fMRI data (Beissner et al. 2014) (Figure 4). Such localized fluctuations can also be clearly seen with a single-slice cine-FLASH (fast low-angle shot) cardiac-gated image of the brainstem at $0.3\times0.3\times1.0$ mm^3 resolution (TR/TE/matrix/bandwidth/FA=129.45 ms/21 ms/$192\times192\times54$ mm^3/223 $HzPx^{-1}$/15°), with example frames shown in Figure 5 (see Supporting Movies S1 and S2). This movie depicts the anatomy of the brainstem and surrounding anatomical structures through retrospectively gating the imaging data and reconstructing the image at 25 evenly-spaced phases of the cardiac cycle.

Based on the observation that the brainstem is surrounded by strong noise sources rather than being affected in its entirety by a “piston-like” motion (as suggested by earlier studies (Poncelet et al. 1992), it became clear that the influence of cardiorespiratory artifacts could be significantly reduced by restricting the analysis to an anatomically-defined brainstem mask (Beissner and Baudrexel 2014; Sclocco et al. 2016; Moher Alsady et al. 2016). The

optimal approach tightly masks the brainstem *prior to* any spatial smoothing, limiting the extension of physiological noise into deeper brainstem nuclei.

2.4 Magnetic susceptibility-induced distortions by air-filled cavities

While increases in ΔR_2* at UHF can help in localizing brainstem nuclei (as noted above), such increases also cause larger susceptibility-induced distortions in EPI-based acquisitions used for fMRI, most prominently in the brainstem region, due to the steep magnetic susceptibility gradient produced by the air-tissue boundary of the posterior part of the oral cavity (Gizewski et al. 2014). This effect can be partially mitigated through the use of accelerated parallel imaging (de Zwart et al. 2006; Griswold et al. 1999), or reduced post-acquisition through corrections based on a field map (Jezzard and Balaban 1995) or other reference data (Andersson et al. 2003). Additionally, through-slice dephasing, due to susceptibility gradients that cause phase dispersion across the slice leading to signal cancellation, grows with magnetic field strength. However, since the drop-out is a function of the spread of phase across the slice, a thinner slice will have a narrower phase distribution in the slice direction and therefore less drop-out. The higher SNR afforded by UHF allows for thinner slices, hence compensating for this effect. Still, residual geometric distortions in EPI images hamper the coregistration of functional to structural images and the transformation to standard space, necessary for multi-subject group analyses. A proposed strategy to overcome this drawback is the use of an anatomical reference dataset with identical distortion to the BOLD fMRI data, such as T_1-weighted EPI data, to assist with the mapping to anatomical reference data or a template (Grabner et al. 2014; Tootell et al. 1997) Renvall et al. recently used anatomical EPI data with 1 mm isotropic voxel size, acquired with a fast multiple inversion recovery time EPI sequence at 7 tesla, in order to calculate quantitative T_1 maps. T_1-weighted data were then synthesized from these maps using the Bloch equations, and automatically segmented using FreeSurfer (Renvall et al. 2016). This approach improved the accuracy of the spatial alignment with the BOLD fMRI data, and has been successfully applied to brainstem fMRI data, where accurate coregistration enabled improved masking of brainstem structures by transforming a brainstem mask defined in MNI space to individual functional space (Sclocco et al. 2016).

2.5 Brainstem probabilistic atlases

Current probabilistic *in vivo* brain atlases (Keuken et al. 2014; Destrieux et al. 2010; Desikan et al. 2006; Tzourio-Mazoyer et al. 2002) released with common neuroimaging software (e.g FSL, FreeSurfer, SPM) include several cortical and subcortical regions, but not most brainstem nuclei nor their subdivisions. Atlases including a limited number of brainstem nuclei, such as the substantia nigra (SN), red nucleus (RN), and subthalamic nucleus (STh) (Keuken et al. 2014; Chowdhury et al. 2013; Kwon et al. 2012; Menke et al. 2010; Mori et al. 2009) do exist, though their subdivisions are not reported. Mori et al. developed and publicly released an *ex vivo* diffusion tensor imaging (DTI) atlas of brainstem white matter tracts (Mori et al. 2008; Mori et al. 2009) and in recent work, this group also showed the feasibility of *ex vivo* DTI imaging of several nuclei important for motor and cranial nerve functional systems in a single postmortem brainstem specimen (Aggarwal et al. 2013).

A recently developed preliminary *in vivo* neuroimaging probabilistic structural atlas has been reported in standard stereotaxic (MNI) space (Bianciardi et al. 2015). This study used 7 tesla MRI and a multi-contrast (diffusion fractional anisotropy and T2-weighted) echo-planar-imaging approach, which provided complementary contrasts for brainstem nuclei anatomy with matched geometric distortions and resolution. Labels of probabilistic brainstem nuclei were generated for the ascending arousal (median and dorsal raphe), autonomic (raphe magnus, periaqueductal gray) and motor (inferior olivary nuclei, two subregions of the substantia nigra compatible with pars compacta and pars reticulata, two subregions of the red nucleus and, in the diencephalon, two subregions of the subthalamic nucleus) systems. These labels may lead to the first step towards the development of a comprehensive in vivo neuroimaging atlas of brainstem nuclei in standard space to facilitate future clinical and research investigations of human brainstem function and pathology. Follow-up studies at 7 tesla have mapped the functional connectivity of these brainstem nuclei labels (Bianciardi et al. 2016) and clinical applications for this brainstem nuclei atlas (traumatic coma) was provided (Bianciardi et al. 2016).

3. Brainstem-based neuromodulatory systems

3.1 The serotonergic system and raphe nuclei

Serotonin (5-hydroxytryptamine or 5-HT) is a monoamine neurotransmitter involved in many different functions within the CNS, acting as a global homeostatic regulator of emotion (Elliott et al. 2011; Hale and Lowry 2011), mood (Sharp and Cowen 2011), nociception (Fields et al. 1977), sleep (Monti 2010), autonomic functions and as a regulator of motor activity (Di Matteo et al. 2008; Heckman et al. 2008). In the brainstem, the highest concentration of serotonergic neurons is found in the raphe nuclei, cell groups extending from the medulla to the midbrain that are clustered throughout the midline. Raphe nuclei are the primary source of serotonergic projections to the forebrain, brainstem, and spinal cord. Medullary raphe nuclei (Ncl. raphe pallidus, obscurus, and magnus) correspond to groups B1, B2, and B3 of Dahlström and Fuxe (Dahlstroem and Fuxe 1964) and are mainly associated with descending spinal projections. Fibers from the nucleus raphe magnus exert an indirect inhibitory action (by inhibiting second order neurons in the spinal cord) upon nociceptive neurons, producing an analgesic effect (Fields et al. 1977). Furthermore, medullary raphe nuclei also inhibit sympathetic preganglionic neurons (Coote 1990). The raphe nuclei in the pons and midbrain (Ncl. raphe pontis, dorsalis, and reticularis centralis superior) are larger than their medullary counterparts. They mainly show ascending projections with their principal fibers arborizing profusely throughout the substantia nigra, periaqueductal gray matter, thalamus, hypothalamus, and cerebral cortex (Parent 1996).

MRI *in vivo* investigation of the raphe nuclei has been severely hampered by the limited sensitivity and contrast between these nuclei and adjacent white matter (Bianciardi et al. 2015). Recently, significant advances have been made by combining high-resolution research tomography (HRRT) positron emission tomography (PET) and UHF MRI techniques. Son and colleagues (Son et al. 2012) successfully exploited fluorodeoxyglucose (FDG) PET imaging to identify four distinct clusters with high metabolic activity located in the brainstem midline region, consistent with putative raphe nuclei. UHF-MRI images were

then fused with the metabolic data to produce a single image with major brainstem anatomical landmarks, which allowed for identification of clusters putatively consistent with the Ncl. raphe dorsalis, pontis, magnus, and reticularis centralis superior. Importantly, a follow-up study from the same group reported significant correlation between the standard uptake of FDG and nondisplaceable binding potential of DASP, a radioligand designed to study the serotonin transporter (Son et al. 2014). Both measures identified a group of clusters consistent with the previous results, but also including the smaller medullary raphe obscurus and pallidus.

Other UHF MRI applications for improved localization of raphe nuclei attempted to combine diffusion imaging measures of fractional anisotropy (FA) with T_2-weighted EPI images with 1.1 mm isotropic resolution, to create *in vivo* probabilistic labels of Ncl. raphe dorsalis, reticularis centralis superior, and raphe magnus (Bianciardi et al. 2015). Through multi-contrast imaging, all three nuclei were identified by their low FA values.

3.2 The noradrenergic system and locus coeruleus

Noradrenaline is a catecholamine widely diffused in the human brain and body, where it functions as a neurotransmitter and hormone, respectively. The locus coeruleus (LC, group A6 of Dahlström and Fuxe) is the largest collection of noradrenergic neurons in the brain. This structure distributes descending and ascending noradrenergic fibers that terminate in virtually all parts of the CNS. Thus, alterations in activity of a small number of LC neurons can have wide influence across functionally diverse regions of the brain. Multiple studies of the LC-noradrenaline system have led to the identification of two general levels of action (reviewed in (Berridge and Waterhouse 2003)). First, LC neurons contribute to activity states amenable to the reception of sensory information (Amatruda et al. 1975; Aston-Jones and Bloom 1981). Second, within the awake state, a variety of higher cognitive and affective processes are modulated by the noradrenergic system, so as to facilitate responding to relevant, salient stimuli while suppressing response to irrelevant stimuli (Foote et al. 1980). More recently, an interaction between tonic and phasic discharges of LC neurons was found, leading to the Adaptive Gain Theory (Aston-Jones and Cohen 2005), which proposes that LC neurons are phasically activated in response to decision outcome. For instance, a recent lower field human fMRI study suggested that phasic LC activation just prior to button press for subjective ratings of increasing stimulus-evoked nausea (Napadow et al. 2013). In contrast, high tonic discharges in LC, measured when task attentiveness wanes, have been interpreted as a mechanism facilitating behavioral flexibility, rather than focused attention (Bouret and Sara 2005).

As is often the case with brainstem nuclei, a key challenge of *in-vivo* LC investigation with MRI is its small cross-sectional area (see Table 1) and the lack of precise information about its normative position in standard space (e.g. MNI). Interestingly, a recent study exploited the presence of neuromelanin, a pigment produced in noradrenergic neurons that exhibits ferrous properties (Enochs et al. 1997), in order to visualize the LC using a T_1-weighted Turbo Spin Echo sequence (Sasaki et al. 2006). This approach was subsequently extended to a larger cohort (N = 44), in order to obtain a probabilistic map of LC in standard MNI space (Keren et al. 2009). Using this region-of-interest to guide localization, a recent 7T fMRI

study found increased temporal correlation between LC fMRI signal and the high-frequency component of heart rate variability, an index of parasympathetic activity, during sustained evoked-pain stimulus (Sclocco et al. 2016). Interestingly, this correlation was significant only during the first 2 minutes of the 6-minute sustained pain stimulus, suggesting a faster, phasic LC response, possibly related to the initial novelty of the nociceptive stimulus. The LC is also a key brainstem nucleus involved in anesthesia (and consciousness) research, specifically implicated in the transition from an anesthesized to an awake state (Leung et al. 2014; Vazey and Aston-Jones 2014). Future research should take advantage of UHF fMRI advances to further probe the role of this nucleus in human anesthesia applications.

3.3 The cholinergic system

Within the reticular formation, neurons containing acetylcholine (ACh) abound particularly in the central portions of the reticular core. In the midbrain, a clinically important cholinergic center is the pedunculopontine nucleus (PPN), corresponding to the CH5 group, as defined by Mesulam and co-authors (Mesulam et al. 1984). The PPN is part of the mesencephalic locomotor region, which also includes the cuneiform and subcuneiform nuclei. It mainly gives rise to ascending projections, particularly to the pars compacta of the substantia nigra and the subthalamic nucleus. Low frequency stimulation of PPN has been shown to elicit walking movements, while lesions of this nucleus result in gait deficits (Karachi et al. 2010). As a result, the PPN has recently received much attention as a target for deep brain stimulation (DBS) techniques in Parkinson's disease, particularly for the treatment of freezing of gait (FOG) when patients respond poorly to dopamine therapy and DBS of the subthalamic nucleus (Ferraye et al. 2010). The exact location of PPN, though, is generally elusive to clinical MRI, and stereotactic atlases usually identify only the rostral component of PPN (Zrinzo et al. 2008). However, new studies suggest the possibility of an increased effectiveness of DBS in the caudal portion (Thevathasan et al. 2012), raising the need for a better anatomical definition of this nucleus (Windels et al. 2015). In this context, UHF MRI could play a pivotal role, providing the enhanced SNR necessary to better identify PPN subregions in patient populations. In particular, a functional mapping approach could be pursued, since the PPN has been shown to be involved in motor planning and activating during imagined gait, unlike the subthalamic nucleus (Lau et al. 2015).

3.4 The dopaminergic system

Dopaminergic cell bodies are confined to the mesencephalic portion of the human brainstem, where they are grouped into two main structures, the substantia nigra (SN) pars compacta (SNc), encompassing groups A8 and A9 of Dahlström and Fuxe, and the ventral tegmental area (VTA), corresponding to group A10. The SN lies dorsally to the crus cerebri, centrally to the midbrain tegmentum, and extends throughout the length of the midbrain. The SNc is an area of densely packed cells that penetrate deep into the pars reticulata (SNr), a cell-poor zone mainly occupied by the striatonigral fibers, and displaying GABA immunoreactivity (Parent 1996).

The ascending projections of these two major dopaminergic nuclei follow two different pathways, the nigrostriatal dopaminergic system, projecting from groups A8/9 to the caudate nucleus and putamen, and the mesolimbocortical system, connecting group A10 with the

ventral striatum, nucleus accumbens, amygdala, and prefrontal cortex (Lavoie et al. 1989). These two pathways are associated to distinct, though overlapping, functions. The nigrostriatal pathway plays a significant role in the control of motor function and in learning new motor skills (Graybiel et al. 1994). A massive loss of pigmented cells of the SNc is a neuropathologic signature of Parkinson's disease (see more in Clinical applications). The mesolimbic dopaminergic system, involving projections from VTA to the nucleus accumbens, has been identified as one of the most important substrates for reward, important for the study of addiction, pain, appetite for food, sex, and social interactions (Koob and Le Moal 2001; Wise 1998). However, recent findings have challenged the primary or exclusive role of dopamine in reward processing (Bromberg-Martin et al. 2010; Salamone and Correa 2012). This is an active field of research, and evidence does still support the primary role of dopaminergic neurons phasic activity in the generation of reward prediction error signals (Schultz 2013). UHF MRI, in conjunction with PET neuroimaging may play a critical role in better understanding this controversy.

3.5 The periaqueductal gray (PAG) and its role in multiple neuromodulatory systems

The PAG is a small (Table 1) yet complex columnar region surrounding the mesencephalic aqueduct with neurons associated with multiple neurotransmitter systems and involved in survival-related responses and homeostatic regulation important for affective responses, nociception, and stress (Bandler et al. 2000). It has no clear cytoarchitectonical boundaries, but evidence suggests an organization into four longitudinal columns parallel with the aqueduct, namely the dorsomedial (dmPAG), dorsolateral (dlPAG), lateral (lPAG) and ventrolateral (vlPAG) (Carrive 1993). Similar efferents are noted for dmPAG, lPAG and vlPAG, which project directly to the lower brainstem. These PAG subregions receive afferents from dorsomedial/orbital prefrontal cortex, cingulate cortex, and central amygdala nucleus. In contrast, dlPAG receives afferent fibers from the medial prefrontal cortex and the basolateral amygdale (An et al. 1998). Additionally, the PAG is organized rostrocaudally. Neurons of lamina I of the superficial dorsal horn and caudal trigeminal nucleus provide nociceptive information to the contralateral PAG. These projections target lPAG and vlPAG and are somatotopically organized: trigeminal projections terminate in the rostral PAG, and cervical and lumbar spinal projections at progressively more caudal levels (Yezierski 1988; Benarroch 2012). This complex cytoarchitecture is paralleled by an equally complex chemoarchitecture. The PAG contains neurons utilizing glutamate, GABA, endogenous opioids (particularly enkephalin), substance P, neurotensin, as well as other neurotransmitters (Benarroch 2012). The vlPAG is suggested to regulate passive defensive behaviors and opioid analgesia, and has a hypotensive effect when stimulated. Furthermore, lPAG and dlPAG stimulation gives rise to "active coping" strategies such as fight/flight behaviors, hypertension, tachycardia and non-opioid mediated analgesia. Stimulation of the vlPAG, on the other hand, evokes "passive coping" behaviors such as quiescence, hypotension, bradycardia, and opioid mediated analgesia (Bandler et al. 2000; Benarroch 2012). A recent 3T fMRI study using resting-state fMRI to investigate functional connectivity in PAG revealed connections between the vlPAG and brain regions associated with descending pain modulation (anterior cingulate cortex, upper pons/medulla), whereas lPAG and dlPAG were connected with brain regions implicated in executive functions (prefrontal cortex, striatum, hippocampus) (Coulombe et al. 2016).

UHF imaging of the PAG, using high spatial resolution methods, holds great promise due to this complex architecture. A recent review bemoaned the great heterogeneity in PAG localization reported in prior neuroimaging publications (Linnman et al. 2012). In fact, this same study also highlighted the lack of specificity of activations reflecting the known columnar organization of the PAG. Specifically, Linnman et al. found no clear separation of average peak activation locations for different stimuli and attributed this lack of differentiation to the limited spatial resolution found for most low field fMRI studies. Indeed, the anatomical and functional characteristics of the PAG – reduced dimension of its highly specified subdivisions, close proximity to the cerebral aqueduct – make this nucleus a perfect candidate for improved imaging at UHF. Satpute and coauthors used UHF fMRI to image the PAG with a 0.75 mm isotropic spatial resolution (Satpute et al. 2013), while exposing participants to emotionally aversive images. Activation was localized to lPAG and dmPAG rostrally, and to vlPAG caudally, consistent with observations from animal studies (Moss and Basbaum 1983; Moss et al. 1983). Analyses on a voxel-by-voxel basis showed peak activations in caudal vlPAG and rostral lPAG, indicating the feasibility of exploring the functional architecture of small, difficult to image nuclei with UHF. More recently, Faull et al. explored the role of PAG in respiratory control using UHF fMRI with 1 mm isotropic voxel size (Faull et al. 2015). Their results show deactivation in lPAG and dmPAG columns during short (around 10 s) breath hold blocks, suggesting the involvement of these PAG subdivisions for conscious respiratory control. In a subsequent study, the same group found evidence of lPAG involvement in resistive respiratory loading, whereas vlPAG was associated to anticipation of breathlessness (Faull et al. 2016).

3.6 Magnetic Resonance Spectroscopy for neurotransmitter assessment

In the brain, γ-aminobutyric acid (GABA) is the major inhibitory transmitter, whereas glutamate (Glu) is the major excitatory transmitter. In contrast to acetylcholine and amines (such as dopamine, noradrenaline, serotonin), which are synthesized only in certain neurons, GABA and Glu play a key role in the regulation of multiple circuitries (see e.g. (Meldrum 2000; Petroff 2002)). Some examples of GABAergic and glutamaternic neurotransmission include the genesis of paradoxical sleep (Luppi et al. 2012) and the signaling from nucleus tractus solitarii (NTS) to Ncl. ambiguus (NAmb), mediating cardiorespiratory reflexes, and to dorsal motor nucleus of the vagus (DMNX) mediating gastric function (Travagli et al. 2006).

The main tool for assessment of GABA and Glu concentration *in vivo* is proton MR spectroscopy (H-MRS). UHF provides significantly improved SNR for MRS techniques and reduces chemical shift dispersion (i.e., multiplets) of single proton peaks, thus allowing for better spectral resolution. However, UHF requires some care in data acquisition for MRS due to limitations in available B_1^+ magnitude and the necessity of using short TEs (see (Tkac and Gruetter 2005)). Due to typical voxel size (in the order of 1cm isotropic) most *in vivo* MRS studies have focused on cortical and subcortical (e.g. thalamus, striatum) regions (Tkac et al. 2009; Terpstra et al. 2010). However, a recent 7 tesla MRS study used a single-voxel approach to assess metabolites in substantia nigra and pons (Emir, Auerbach, et al. 2012). Results showed relatively high GABA levels in the substantia nigra, as well as high choline in the pons, consistent with the known biochemistry of these regions, supporting the

feasibility of MRS investigation in the brainstem. The same group applied UHF MRS to assess brainstem metabolite concentration for Parkinson's disease (PD) (Emir, Tuite, et al. 2012), known to be characterized by degeneration of nigrostriatal dopaminergic neurons. A preliminary comparison revealed GABA elevation in the pons relative to putamen in PD patients, consistent with earlier pathological involvement of the brainstem, and suggesting a potential biomarker for disease staging (Emir, Tuite, et al. 2012).

4. Assessing specific brainstem neural circuitries with UHF MRI: pain processing and autonomic control

4.1 Neuroimaging brainstem nociceptive circuitry

Nociception is defined as the sensory nervous system's response to potentially harmful stimuli. The central processing of such response is responsible for the perception of pain. Descending control of spinal nociceptive afference involves multiple brain regions and plays a major role in determining the experience of both acute and chronic pain. Earlier studies identified the inhibitory influence of a brainstem network involving the midbrain periaqueductal gray (PAG), as well as a functionally defined rostral ventromedial medulla (RVM) region, which includes the nucleus raphe magnus and adjacent reticular regions (Basbaum and Fields 1978; Fields and Basbaum 1978; Basbaum and Fields 1984). This PAG-RVM axis has been regarded as the source of descending inhibitory control of pain, contributing to anti-nociceptive mechanisms under extreme stress (Terman et al. 1984), or selectively inhibiting ascending non-nociceptive information in presence of nociceptive information, to enhance the signaling of pain (Le Bars 2002). Subsequent studies also described a pain facilitatory circuitry including the same brain regions (Zhuo and Gebhart 1997). The opioid antagonist naloxone has been used to investigate the opioidergic mechanisms underlying placebo analgesia. Combining naloxone with fMRI at 3 tesla, Eippert and colleagues observed reduced placebo-induced responses in key structures of the descending pain control system, including PAG and RVM (Eippert et al. 2009).

The different PAG columns (see section 3.5) receive functionally segregated inputs from nociceptive pathways. Afferents from superficial nociceptors are conveyed to the lPAG and dlPAG columns (mainly via Aδ-fibers). The vlPAG receives inputs from visceral, muscle and C-fiber skin nociceptors, as well as visceral inputs from the nucleus tractus solitarii and the sacral spinal cord (Parry et al. 2008; Benarroch 2012).

Decades of investigation on the neuronal populations of RVM have led to the classification of so-called ON, OFF, and NEUTRAL classes of neurons. The OFF-cells are silent during nociceptive withdrawal (Fields, Bry, et al. 1983), and were found to be responsible for anti-nociceptive output from the RVM (Heinricher and Ingram 2008). Subsequently, growing evidence on the pain facilitatory role of RVM stemmed from the observation that behavioral hyperalgesia was correlated with increased activity of ON-cells (Fields, Vanegas, et al. 1983). Importantly, these cells were defined in animals and are anatomically intermingled; thus, activity cannot be separated with conventional MRI imaging approaches in humans.

In addition to the PAG-RVM system, other medullary regions, namely the dorsal reticular nucleus (DRt) and the caudal lateral ventrolateral medulla (VLM), have also been implicated in descending pain control (Lima and Almeida 2002; Foong and Duggan 1986; Gebhart and Ossipov 1986). However, the presence of documented ON- and OFF-cells in the VLM points to a dual inhibitory/facilitatory role, similar to RVM (Pertovaara and Almeida 2006). A recent study linked conditioned pain modulation analgesia to a reduced fMRI signal in the caudal spinal trigeminal nucleus (Sp5), DRt and dorsolateral pons (Youssef et al. 2014). Other midbrain nuclei also participate in descending inhibition/facilitation. The nucleus cuneiformis (NCF) is involved in both ascending transmission and modulation of nociceptive afference. It also contains ON/OFF cells (Haws et al. 1989) and like the PAG projects to the RVM. Previous neuroimaging studies at 3 tesla have shown that NCF and RVM fMRI responses to pain are correlated (Dunckley et al. 2005), and that NCF is involved in modulating pain intensity by expectancy effects (Keltner et al. 2006).

In fact, pain-related PAG fMRI activity has been consistently reported at lower field strengths (Linnman et al. 2012), although with the limitations discussed above. Recently, Hahn et al. compared fMRI responses to painful versus innocuous electrical stimulation at 3 and 7 tesla (Hahn et al. 2013), adopting similar in-plane resolutions for both field strengths (1.48×1.48 mm^2 at 3 tesla, 1.5×1.5 mm^2 at 7 tesla), and found that PAG activation for painful versus innocuous stimulation was found only with UHF fMRI. These results support a potentially important role of UHF fMRI in evaluating brainstem nociceptive circuitries. Future studies should combine UHF fMRI with optimized imaging and processing approaches, to take advantage of high spatial resolution and disambiguate the function of NCF and PAG, and target the medullary components (RVM, DRt, VLM) of descending pain modulation.

4.2 The central autonomic network (CAN)

The autonomic nervous system (ANS) is involved in virtually every aspect of daily life. The motor arm of the ANS regulates physiology within a variety of systems including respiratory, cardiac, vasomotor, digestive, and endocrine. This ANS outflow calibrates bodily reactions with contextually adaptive behavior to meet the metabolic demands of motor, emotional, and cognitive challenges (see for example (Thayer and Lane 2000; Critchley 2005). In order to maintain homeostasis, the activity of spinal (preganglionic) neurons is continuously regulated by higher levels in the brain. The CNS regions involved in this control system are known as the central autonomic network (CAN), including mid-cingulate, insula, and ventromedial prefrontal cortices, thalamus, hypothalamus, and amygdala (Beissner et al. 2013).

In the brainstem, the nucleus tractus solitarii (NTS) receives afference via vagal, glossopharyngeal, and facial nerves. The NTS extends rostrally to the lower border of the pons, while caudally it merges with the contralateral column below the obex. It receives afference from the vagus nerve, and extends glutamatergic influence to premotor cardiovagal neurons in the nucleus ambiguus (NAmb) and, to a lesser extent, in the dorsal motor nucleus of the vagus (DMNX) (Neff et al. 1998). This interaction has been demonstrated only in animal models and should be explored in humans with the aid of UHF fMRI. The NTS/

NAmb link is also influenced by tonic inhibitory influence from arcuate and paraventricular (PVN) hypothalamic nuclei onto NAmb (Ciriello et al. 2003; Chitravanshi et al. 2015), forming the core central control circuitry for cardiovagal modulation. Furthermore, NTS and NAmb, as well as surrounding portions of the medullary reticular formation, have been physiologically defined as the dorsal medullary respiratory center (Kalia 1977), in addition to the Kölliker-Fuse nucleus in the pons and portions of the PAG in the midbrain (see section 3.5). It is well-known that breathing introduces rhythmic oscillations in cardiovascular physiology for optimal oxygen diffusion (Wehrwein and Joyner 2013). This respiratory sinus arrhythmia (RSA) occurs by modulation of premotor cardiovagal neurons (e.g. NAmb) by diverse mechanisms, including afference (via NTS) from the lungs and thoracic baroreceptors, as well as direct input from medullary respiratory neurons (Dergacheva et al. 2010; Wehrwein and Joyner 2013; Zoccal et al. 2014). NTS neurons play an essential role in coordinating RSA by modulating premotor cardiovagal sympathetic outflow from NAmb and the rostral ventrolateral medulla (rVLM) (Spyer 1981; Schreihofer and Guyenet 2003).

The *in vivo* MRI localization of the aforementioned autonomic nuclei has been very challenging with standard structural T1 or T2-weighted scans due to the lack of contrasts between these cell columns and the surrounding tissues. However, recent functional MRI approaches (at 3 tesla with 2.5mm in-plane resolution) have reported activation of dorsal and lateral medulla in response to CO_2 stimulation (Pattinson et al. 2009). Given the available spatial resolution, a medullary cluster encompassing several nuclei was identified, leaving the exact localization of specific cell groups uncertain. UHF fMRI could substantially improve localization for such applications. An alternative approach to functional localization is adopting stimulation paradigms known to modulate the autonomic nervous system, and using peripheral autonomic signals to guide analysis of fMRI data. Recent studies have used an instantaneous estimation of parasympathetic outflow (Barbieri et al. 2005) as an independent variable in general linear model analysis of fMRI data during hand grip (Napadow et al. 2008), visually-induced nausea (Sclocco et al. 2014), and, using 7 tesla fMRI, continuous pain (Sclocco et al. 2016). Similarly, Macefield and Henderson recently evaluated brainstem activity by recording fMRI signals (at 3 tesla with 1.5mm in-plane resolution, TR=8s) concurrently with spontaneous fluctuations in muscle sympathetic nerve activity (MSNA), collected using microneurography in awake humans at rest (Macefield and Henderson 2010). Results suggested that small increases in MSNA were associated with fMRI signal increases in the rVLM, whereas decreases occurred in the central VLM (cVLM), as well as NTS. Future applications should take advantage of multi-band techniques at UHF to couple fMRI data collected with both small voxel size and short TR for better assessment of central autonomic network control circuitry.

5. Clinical applications

Noninvasive clinical testing of the integrity of relevant brainstem centers would be a highly desirable diagnostic tool for a myriad of disorders, such as those characterized by autonomic failure, Parkinson’s disease, affective disorders, sleep disorders, and chronic pain. Furthermore, a better understanding of brainstem function is a prerequisite for developing novel therapeutic strategies for the treatment of such disorders (Beissner 2015). Lesions or pathological variations affecting the brainstem often produce numerous and severe clinical

deficits owing to the fundamental role played by the brainstem in CNS physiology. The past few years have seen a number of important advances that bring us closer to routine application of this method in the clinical setting.

5.1 Invasive and non-invasive neuromodulation for chronic pain

The involvement of the brainstem in pain and nociceptive processing makes this structure a major target for the treatment of chronic pain. In particular, invasive clinical approaches such as deep brain stimulation (DBS) of the sensory thalamus have been used for the treatment of pain and co-morbid depression for more than fifty years (Duncan et al. 1991), and DBS of the PAG and periventricular gray (PVG) is still adopted in refractory syndromes, such as phantom limb pain (Bittar et al. 2005). Despite its clinical usage, detailed with a significant body of literature, the neurophysiological and neurochemical basis of the beneficial effects of PAG/PVG DBS is still controversial. The initial hypothesis of an opioid-mediated analgesia (Hosobuchi et al. 1977) was challenged by subsequent studies showing that PAG/PVG electro-analgesia is not fully blocked with the opioid antagonist naloxone (Duncan et al. 1991). Interestingly, a recent study addressed this open issue with [^{11}C]diprenorphine (DPN, an opioid radioligand) PET in a small cohort of patients with implanted PAG/PVG DBS systems. The results showed a significant decrease in [^{11}C]DPN binding in the caudal, dorsal PAG following DBS from effective electrodes located in rostral dlPAG, thus suggesting a focal release of opioid peptides (Sims-Williams et al. 2016). However, as PET ligands assess only a single neuromodulatory system, whether this endogenous opioid release is playing the most significant role in analgesia still needs to be determined. Due to the existence of both inhibitory and facilitatory projections from PAG, the effects of DBS are different depending on the target area. An important contribution of UHF fMRI in this context could be improved spatial resolution for a better mapping of different PAG subdivisions, in order to better determine the desired response. Additionally, as target brainstem nuclei have very small cross-sectional area, UHF MRI may play an important role in pre-surgical planning and MR-guided surgery for precise lead placement (Chansakul et al. 2016), though clinical benefits of 7 tesla MRI have yet to be seen for DBS of the brainstem (van Laar et al. 2016).

Non-invasive neuromodulatory approaches for pain have also targeted brainstem nuclei by electrically stimulating cranial nerves. One promising approach is the targeting of NTS with transcutaneous vagus nerve stimulation (tVNS). Vagus Nerve Stimulation (VNS), which involves surgical placement of electrodes coiled around the cervical vagus nerve within the carotid sheath, has demonstrated efficacy for multiple disorders (e.g. epilepsy, depression), and recently, migraine (Hord et al. 2003; Mosqueira et al. 2013; Yuan and Silberstein 2015). Despite the therapeutic potential of VNS, adverse events and complications associated with surgery and chronic stimulation limit broad applicability (Fahy 2010). Importantly, the NTS and Sp5 also receive somatosensory afference via the auricular branch of the vagus nerve (ABVN) (Nomura and Mizuno 1984; Kiyokawa et al. 2014). Non-invasive (transcutaneous) methods of ABVN stimulation (tVNS) have been proposed (Ventureyra 2000), and preliminary 3T neuroimaging studies have found that tVNS modulates brainstem and cortical areas similar to classical VNS (Frangos et al. 2015; Dietrich et al. 2008; Kraus et al. 2013), while a clinical trial suggested that tVNS may also reduce the frequency of migraine

episodes (Straube et al. 2015). Interestingly, the dorsal medullary vagal system operates in tune with respiration (see above) and ABVN stimulation gated to exhalation may optimize tVNS outcomes (Napadow et al. 2012). Importantly, while the challenges of brainstem fMRI have limited the number of studies in migraine and other chronic pain patients, existing imaging studies have shown interictal abnormalities in migraneurs in subcortical and brainstem regions responsible for somatosensory processing (Harriott and Schwedt 2014; Akerman et al. 2011; Mainero et al. 2011; Moulton et al. 2008; Moulton et al. 2014). For instance, a recent 3 tesla fMRI study found that Sp5 response to tactile stimuli in migraine was amplified in higher cortical regions and sensitive to interictal phase (Lee et al. 2016). Neuromodulatory interventions, such as tVNS, may target specific brainstem nuclei such as NTS and the trigeminal sensory pathway, as also suggested in a recent tVNS fMRI study (Garcia et al. 2016), to ameliorate migraine pathophysiology. In fact, NTS response to ABVN electrical stimulation may be more focally identified with UHF fMRI, and future neuroimaging studies could use cranial nerve stimulation techniques such as tVNS (known to target distinct medullary nuclei), with a goal to optimize UHF fMRI brainstem-focused pulse sequence development.

5.2 UHF applications for Parkinson's disease

The diagnosis of Parkinson's disease (PD) is by far the most explored clinical application of UHF MRI. Parkinson's disease is characterized by rhythmic tremor at rest, increased muscle tone or rigidity, and slowness in the initiation and execution of movements. It is estimated that the percentage loss of dopaminergic neurons in the substantia nigra (SN) exceeds 60% before a patient shows any clinical symptoms (Hornykiewicz and Kish 1987; Riederer and Wuketich 1976), therefore the possibility of examining the midbrain SN *in vivo* in the human has been one of the most sought-after goals in Parkinson's research (Lang and Lozano 1998; Hughes et al. 1992; Meara et al. 1999). Given the melanin content of the SNc and the higher levels of iron of the SNr (Morris et al. 1992), the increased CNR and spatial resolution offered by UHF MRI has significantly advanced the capabilities of detecting pathological changes in SN morphology (for a recent review, see (Lehericy et al. 2014)). The first successful UHF studies of SN degeneration in PD detected pockets of high signal intensity in the dorsolateral part of the SN (Cho et al. 2011; Kwon et al. 2012; Cosottini et al. 2014), that were subsequently identified as nigrosome-1 (Blazejewska et al. 2013). This same study also confirmed that the SNr and SNc can be distinguished on the basis of MRI signal (SNr is hypointense in T_2-weighted images, and hyperintense in T_1-weighted images) (Blazejewska et al. 2013). More recently, a 7 tesla study found this T1 hyperintensity to be lost in PD, multiple system atrophy, and progressive supranuclear palsy (Blazejewska et al. 2015). Such promising applications can hopefully lead to clinical incorporation to diagnose and track neurodegeneration in PD patients.

6. Future directions

An *in vivo* structural delineation of most human brainstem nuclei (similar to existing probabilistic atlases for the cortex and higher subcortical regions) has been in great need but elusive because of limited sensitivity and contrast for detecting these small regions using standard neuroimaging methods (see also Section 2.5). 7 tesla brainstem nuclei atlases

(generated in MNI space) could be used similarly to other brain neuroimaging atlases in MNI space (e.g. AAL, Harvard Oxford (Desikan et al. 2006; Tzourio-Mazoyer et al. 2002)), i.e. by co-registering the MNI space (and therefore the 7 tesla brainstem nuclei atlas) to single-subject 3 tesla images (or vice-versa).

Another future application for UHF brainstem MRI will be to incorporate such methods with non-human primate research, as recently demonstrated (Zitella et al. 2015), allowing for more precise neurophysiological experimentation to better understand the systems detailed in our review above.

Finally, development of better neurovascular coupling hemodynamic response models is likely to play an important role in UHF brainstem fMRI. The assumption of a spatially homogeneous hemodynamic response function (HRF) has been repeatedly challenged in the literature (Handwerker et al. 2004; Aguirre et al. 1998), and more complex basis sets have been introduced in order to account for such variability (see for example (Lindquist et al. 2009)). However, the performance of the most widely adopted methods, such as derivative and related models, has been shown to be biased for temporal shifts greater than a few seconds from the canonical response (Lindquist et al. 2009). In addition, the high spatial resolution afforded by UHF has been recently highlighted as a potential cause of bias for current BOLD models. In fact, collecting signals from different vascular compartments, or cortical layers and columns, in *separate* voxels, translates into the necessity of modeling different processes that were previously merged into a single voxel (Goense et al. 2016). Furthermore, recent accounts from optical imaging and two-photon microscopy suggest that blood flow regulation may be much tighter and more specific to neuronal activity than previously believed. Indeed, several groups now are observing functional activation differences within subcortical nuclei and even between the feeding arterioles and the distribution of the control structures on the vessels – which, given recent investigations of vessel diameter regulation via pericytes, could be present on the capillaries themselves (O'Herron et al. 2016). This increased specificity, however, should be considered alongside our evolving understanding of the spatial inhomogeneity in the BOLD point-spread function, which appears to vary with cortical depth (Polimeni et al. 2010).

In conclusion, the brainstem is a rich and maddeningly complex structure at the base of the brain whose neuroanatomy and neurophysiology may be best assessed with the aid of recent developments in UHF MRI, as discussed in this review. With wider access to UHF MRI, we anticipate even more advances in our understanding of the role the brainstem plays in directing and facilitating central nervous system function.

Supplementary Material

Refer to Web version on PubMed Central for supplementary material.

Acknowledgments

We sincerely thank Dr. Lawrence Wald for his support and useful discussions, as well as Drs. Boris Keil, Thomas Witzel, and Cris LaPierre for supporting hardware and software developments for 7T fMRI.

Funding

We thank the following organizations for funding support: US National Institutes of Health (NIH), Office Of The Director (OT2-OD023867), National Institute of Biomedical Imaging and Bioengineering (NIBIB), NIH: K01-EB019474 (MB), K01-EB011498 (JRP), R01-EB019437 (JRP), Center for Functional Neuroimaging Technologies P41-EB015896 (RS, MB, JRP, VN); National Center for Complementary and Integrative Health (NCCIH), NIH: R61-AT009306 (VN), P01-AT006663 (VN), R01-AT007550 (VN); National Institute of Mental Health (NIMH), NIH: R21-MH103468 (VN); National Institute for Arthritis and Musculoskeletal and Skin Diseases (NIAMS), NIH: R01-AR064367 (VN); National Institute of Neurological Disorders and Stroke (NINDS), NIH: R21-MH103468 (VN). This work also involved the use of instrumentation supported by the NIH Shared Instrumentarium Grant Program and/or High-End Intrumentation Grant Program; specifically, grant nos. S10-RR023034 and S10-RR023401.

References

Afshar, F., Watkins, F., Yap, JC. Stereotaxic atlas of the human brainstem and cerebellar nuclei: a variability study. Raven Press; 1978.

Aggarwal M, Kageyama Y, Li X, van Zijl PC. B0 -orientation dependent magnetic susceptibility-induced white matter contrast in the human brainstem at 11.7T. Magnetic Resonance in Medicine. 2016; 75:2455–63. [PubMed: 27018784]

Aggarwal M, Zhang J, Pletnikova O, Crain B, Troncoso J, Mori S. Feasibility of creating a high-resolution 3D diffusion tensor imaging based atlas of the human brainstem: a case study at 11.7 T. NeuroImage. 2013; 74:117–27. [PubMed: 23384518]

Aguirre GK, Zarahn E, D'Esposito M. The variability of human, BOLD hemodynamic responses. NeuroImage. 1998; 8:360–9. [PubMed: 9811554]

Akerman S, Holland PR, Goadsby PJ. Diencephalic and brainstem mechanisms in migraine. Nat Rev Neurosci. 2011; 12:570–84. [PubMed: 21931334]

Amatruda TT 3rd, Black DA, McKenna TM, McCarley RW, Hobson JA. Sleep cycle control and cholinergic mechanisms: differential effects of carbachol injections at pontine brain stem sites. Brain Res. 1975; 98:501–15. [PubMed: 1182534]

An X, Bandler R, Ongur D, Price JL. Prefrontal cortical projections to longitudinal columns in the midbrain periaqueductal gray in macaque monkeys. J Comp Neurol. 1998; 401:455–79. [PubMed: 9826273]

Andersson JL, Skare S, Ashburner J. How to correct susceptibility distortions in spin-echo echo-planar images: application to diffusion tensor imaging. NeuroImage. 2003; 20:870–88. [PubMed: 14568458]

Aston-Jones G, Bloom FE. Activity of norepinephrine-containing locus coeruleus neurons in behaving rats anticipates fluctuations in the sleep-waking cycle. J Neurosci. 1981; 1:876–86. [PubMed: 7346592]

Aston-Jones G, Cohen JD. An integrative theory of locus coeruleus-norepinephrine function: adaptive gain and optimal performance. Annu Rev Neurosci. 2005; 28:403–50. [PubMed: 16022602]

Baker KG, Halliday GM, Halasz P, Hornung JP, Geffen LB, Cotton RG, Tork I. Cytoarchitecture of serotonin-synthesizing neurons in the pontine tegmentum of the human brain. Synapse. 1991; 7:301–20. [PubMed: 2042112]

Bandler R, Keay KA, Floyd N, Price J. Central circuits mediating patterned autonomic activity during active vs. passive emotional coping. Brain Res Bull. 2000; 53:95–104. [PubMed: 11033213]

Barbieri, Riccardo, Matten, Eric C., Alabi, Abdulrasheed A., Brown, Emery N. A point-process model of human heartbeat intervals: new definitions of heart rate and heart rate variability. American Journal of Physiology Heart and Circulatory Physiology. 2005; 288:H424–35. [PubMed: 15374824]

Basbaum AI, Fields HL. Endogenous pain control mechanisms: review and hypothesis. Ann Neurol. 1978; 4:451–62. [PubMed: 216303]

Basbaum AI, Fields HL. Endogenous pain control systems: brainstem spinal pathways and endorphin circuitry. Annu Rev Neurosci. 1984; 7:309–38. [PubMed: 6143527]

Beissner F. Functional MRI of the Brainstem: Common Problems and their Solutions. Clin Neuroradiol. 2015; 25(Suppl 2):251–7. [PubMed: 25981409]

Beissner F, Deichmann R, Baudrexel S. fMRI of the brainstem using dual-echo EPI. NeuroImage. 2011; 55:1593–9. [PubMed: 21256220]

Beissner F, Schumann A, Brunn F, Eisentrager D, Bar KJ. Advances in functional magnetic resonance imaging of the human brainstem. NeuroImage. 2014; 86:91–8. [PubMed: 23933038]

Beissner, Florian, Baudrexel, Simon. Investigating the human brainstem with structural and functional MRI. Frontiers in Human Neuroscience. 2014; 8:116. [PubMed: 24616692]

Beissner, Florian, Meissner, Karin, Bär, Karl-Jürgen, Napadow, Vitaly. The autonomic brain: an activation likelihood estimation meta-analysis for central processing of autonomic function. The Journal of Neuroscience: The Official Journal of the Society for Neuroscience. 2013; 33:10503–11. [PubMed: 23785162]

Benarroch EE. Periaqueductal gray: an interface for behavioral control. Neurology. 2012; 78:210–7. [PubMed: 22249496]

Berg D, Becker G, Zeiler B, Tucha O, Hofmann E, Preier M, Benz P, Jost W, Reiners K, Lange KW. Vulnerability of the nigrostriatal system as detected by transcranial ultrasound. Neurology. 1999; 53:1026–31. [PubMed: 10496262]

Berridge CW, Waterhouse BD. The locus coeruleus-noradrenergic system: modulation of behavioral state and state-dependent cognitive processes. Brain Res Brain Res Rev. 2003; 42:33–84. [PubMed: 12668290]

Bianciardi M, Toschi N, Edlow BL, Eichner C, Setsompop K, Polimeni JR, Brown EN, Kinney HC, Rosen BR, Wald LL. Toward an In Vivo Neuroimaging Template of Human Brainstem Nuclei of the Ascending Arousal, Autonomic, and Motor Systems. Brain Connect. 2015; 5:597–607. [PubMed: 26066023]

Bianciardi M, Toschi N, Eichner C, Polimeni JR, Setsompop K, Brown EN, Hamalainen MS, Rosen BR, Wald LL. In vivo functional connectome of human brainstem nuclei of the ascending arousal, autonomic, and motor systems by high spatial resolution 7-Tesla fMRI. MAGMA. 2016; 29:451–62. [PubMed: 27126248]

Bianciardi M, van Gelderen P, Duyn JH. Investigation of BOLD fMRI resonance frequency shifts and quantitative susceptibility changes at 7 T. Human Brain Mapping. 2014; 35:2191–205. [PubMed: 23897623]

Bilgic B, Pfefferbaum A, Rohlfing T, Sullivan EV, Adalsteinsson E. MRI estimates of brain iron concentration in normal aging using quantitative susceptibility mapping. NeuroImage. 2012; 59:2625–35. [PubMed: 21925274]

Bittar RG, Otero S, Carter H, Aziz TZ. Deep brain stimulation for phantom limb pain. J Clin Neurosci. 2005; 12:399–404. [PubMed: 15925769]

Blazejewska AI, Al-Radaideh AM, Wharton S, Lim SY, Bowtell RW, Constantinescu CS, Gowland PA. Increase in the iron content of the substantia nigra and red nucleus in multiple sclerosis and clinically isolated syndrome: a 7 Tesla MRI study. J Magn Reson Imaging. 2015; 41:1065–70. [PubMed: 24841344]

Blazejewska AI, Schwarz ST, Pitiot A, Stephenson MC, Lowe J, Bajaj N, Bowtell RW, Auer DP, Gowland PA. Visualization of nigrosome 1 and its loss in PD: pathoanatomical correlation and in vivo 7 T MRI. Neurology. 2013; 81:534–40. [PubMed: 23843466]

Bodurka J, Ye F, Petridou N, Murphy K, Bandettini PA. Mapping the MRI voxel volume in which thermal noise matches physiological noise–implications for fMRI. NeuroImage. 2007; 34:542–9. [PubMed: 17101280]

Bouret S, Sara SJ. Network reset: a simplified overarching theory of locus coeruleus noradrenaline function. Trends Neurosci. 2005; 28:574–82. [PubMed: 16165227]

Boxerman JL, Hamberg LM, Rosen BR, Weisskoff RM. MR contrast due to intravascular magnetic susceptibility perturbations. Magnetic Resonance in Medicine. 1995; 34:555–66. [PubMed: 8524024]

Bromberg-Martin ES, Matsumoto M, Hikosaka O. Dopamine in motivational control: rewarding, aversive, and alerting. Neuron. 2010; 68:815–34. [PubMed: 21144997]

Brooks JC, Faull OK, Pattinson KT, Jenkinson M. Physiological noise in brainstem FMRI. Frontiers in Human Neuroscience. 2013; 7:623. [PubMed: 24109446]

Büttner-Ennever, Jean A., Horn, Anja KE. Olszewski and Baxter's Cytoarchitecture of the Human Brainstem. Eur Surg Res. 2013; 51:101–92. [PubMed: 24217574]

Chang C, Raven EP, Duyn JH. Brain-heart interactions: challenges and opportunities with functional magnetic resonance imaging at ultra-high field. Philos Trans A Math Phys Eng Sci. 2016; 374

Chansakul T, Chen PN Jr, Lee TC, Tierney T. Interventional MR Imaging for Deep-Brain Stimulation Electrode Placement. Radiology. 2016:151136.

Chitravanshi, Vineet C., Kawabe, Kazumi, Sapru, Hreday N. GABA and glycine receptors in the nucleus ambiguus mediate tachycardia elicited by chemical stimulation of the hypothalamic arcuate nucleus. American Journal of Physiology Heart and Circulatory Physiology. 2015; 309:H174–84. [PubMed: 25957221]

Cho ZH, Kang CK, Son YD, Choi SH, Lee YB, Paek SH, Park CW, Chi JG, Calamante F, Law M, Kim YB. Pictorial review of in vivo human brain: from anatomy to molecular imaging. World Neurosurg. 2014; 82:72–95. [PubMed: 23103260]

Cho ZH, Oh SH, Kim JM, Park SY, Kwon DH, Jeong HJ, Kim YB, Chi JG, Park CW, Huston J 3rd, Lee KH, Jeon BS. Direct visualization of Parkinson's disease by in vivo human brain imaging using 7.0T magnetic resonance imaging. Mov Disord. 2011; 26:713–8. [PubMed: 21506148]

Chowdhury R, Lambert C, Dolan RJ, Duzel E. Parcellation of the human substantia nigra based on anatomical connectivity to the striatum. NeuroImage. 2013; 81:191–8. [PubMed: 23684858]

Ciriello, John, McMurray, Jordana C., Babic, Tanja, de Oliveira, Cleusa VR. Collateral axonal projections from hypothalamic hypocretin neurons to cardiovascular sites in nucleus ambiguus and nucleus tractus solitarius. Brain Research. 2003; 991:133–41. [PubMed: 14575885]

Coote JH. Bulbospinal serotonergic pathways in the control of blood pressure. J Cardiovasc Pharmacol. 1990; 15(Suppl 7):S35–41. [PubMed: 1702485]

Cosottini M, Frosini D, Pesaresi I, Costagli M, Biagi L, Ceravolo R, Bonuccelli U, Tosetti M. MR imaging of the substantia nigra at 7 T enables diagnosis of Parkinson disease. Radiology. 2014; 271:831–8. [PubMed: 24601752]

Coulombe MA, Erpelding N, Kucyi A, Davis KD. Intrinsic functional connectivity of periaqueductal gray subregions in humans. Human Brain Mapping. 2016; 37:1514–30. [PubMed: 26821847]

Critchley HD. Neural mechanisms of autonomic, affective, and cognitive integration. J Comp Neurol. 2005; 493:154–66. [PubMed: 16254997]

Dahlstroem A, Fuxe K. Evidence for the Existence of Monoamine-Containing Neurons in the Central Nervous System. I. Demonstration of Monoamines in the Cell Bodies of Brain Stem Neurons. Acta Physiol Scand Suppl. 1964; (SUPPL 232):1–55.

de Zwart JA, van Gelderen P, Golay X, Ikonomidou VN, Duyn JH. Accelerated parallel imaging for functional imaging of the human brain. NMR Biomed. 2006; 19:342–51. [PubMed: 16705634]

Deistung A, Schafer A, Schweser F, Biedermann U, Gullmar D, Trampel R, Turner R, Reichenbach JR. High-Resolution MR Imaging of the Human Brainstem In vivo at 7 Tesla. Frontiers in Human Neuroscience. 2013; 7:710. [PubMed: 24194710]

Dergacheva, Olga, Griffioen, Kathleen J., Neff, Robert A., Mendelowitz, David. Respiratory modulation of premotor cardiac vagal neurons in the brainstem. Respiratory Physiology & Neurobiology. 2010; 174:102–10. [PubMed: 20452467]

Desikan RS, Segonne F, Fischl B, Quinn BT, Dickerson BC, Blacker D, Buckner RL, Dale AM, Maguire RP, Hyman BT, Albert MS, Killiany RJ. An automated labeling system for subdividing the human cerebral cortex on MRI scans into gyral based regions of interest. NeuroImage. 2006; 31:968–80. [PubMed: 16530430]

Destrieux C, Fischl B, Dale A, Halgren E. Automatic parcellation of human cortical gyri and sulci using standard anatomical nomenclature. NeuroImage. 2010; 53:1–15. [PubMed: 20547229]

Di Matteo V, Pierucci M, Esposito E, Crescimanno G, Benigno A, Di Giovanni G. Serotonin modulation of the basal ganglia circuitry: therapeutic implication for Parkinson's disease and other motor disorders. Prog Brain Res. 2008; 172:423–63. [PubMed: 18772045]

Dietrich S, Smith J, Scherzinger C, Hofmann-Preiss K, Freitag T, Eisenkolb A, Ringler R. A novel transcutaneous vagus nerve stimulation leads to brainstem and cerebral activations measured by functional MRI. Biomed Tech (Berl). 2008; 53:104–11. [PubMed: 18601618]

Duncan GH, Bushnell MC, Marchand S. Deep brain stimulation: a review of basic research and clinical studies. Pain. 1991; 45:49–59. [PubMed: 1861878]

Dunckley P, Wise RG, Fairhurst M, Hobden P, Aziz Q, Chang L, Tracey I. A comparison of visceral and somatic pain processing in the human brainstem using functional magnetic resonance imaging. J Neurosci. 2005; 25:7333–41. [PubMed: 16093383]

Eippert F, Bingel U, Schoell ED, Yacubian J, Klinger R, Lorenz J, Buchel C. Activation of the opioidergic descending pain control system underlies placebo analgesia. Neuron. 2009; 63:533–43. [PubMed: 19709634]

Elliott R, Zahn R, Deakin JF, Anderson IM. Affective cognition and its disruption in mood disorders. Neuropsychopharmacology: Official Publication of the American College of Neuropsychopharmacology. 2011; 36:153–82. [PubMed: 20571485]

Emir UE, Auerbach EJ, Van De Moortele PF, Marjanska M, Ugurbil K, Terpstra M, Tkac I, Oz G. Regional neurochemical profiles in the human brain measured by (1)H MRS at 7 T using local B(1) shimming. NMR Biomed. 2012; 25:152–60. [PubMed: 21766380]

Emir UE, Tuite PJ, Oz G. Elevated pontine and putamenal GABA levels in mild-moderate Parkinson disease detected by 7 tesla proton MRS. PloS One. 2012; 7:e30918. [PubMed: 22295119]

Enochs WS, Petherick P, Bogdanova A, Mohr U, Weissleder R. Paramagnetic metal scavenging by melanin: MR imaging. Radiology. 1997; 204:417–23. [PubMed: 9240529]

Fahy BG. Intraoperative and perioperative complications with a vagus nerve stimulation device. J Clin Anesth. 2010; 22:213–22. [PubMed: 20400010]

Faull OK, Jenkinson M, Clare S, Pattinson KT. Functional subdivision of the human periaqueductal grey in respiratory control using 7 tesla fMRI. NeuroImage. 2015; 113:356–64. [PubMed: 25703831]

Faull OK, Jenkinson M, Ezra M, Pattinson KT. Conditioned respiratory threat in the subdivisions of the human periaqueductal gray. Elife. 2016; 5

Ferraye MU, Debu B, Fraix V, Goetz L, Ardouin C, Yelnik J, Henry-Lagrange C, Seigneuret E, Piallat B, Krack P, Le Bas JF, Benabid AL, Chabardes S, Pollak P. Effects of pedunculopontine nucleus area stimulation on gait disorders in Parkinson's disease. Brain: A Journal of Neurology. 2010; 133:205–14. [PubMed: 19773356]

Fields HL, Basbaum AI. Brainstem control of spinal pain-transmission neurons. Annu Rev Physiol. 1978; 40:217–48. [PubMed: 205165]

Fields HL, Basbaum AI, Clanton CH, Anderson SD. Nucleus raphe magnus inhibition of spinal cord dorsal horn neurons. Brain Res. 1977; 126:441–53. [PubMed: 861731]

Fields HL, Bry J, Hentall I, Zorman G. The activity of neurons in the rostral medulla of the rat during withdrawal from noxious heat. J Neurosci. 1983; 3:2545–52. [PubMed: 6317812]

Fields HL, Vanegas H, Hentall ID, Zorman G. Evidence that disinhibition of brain stem neurones contributes to morphine analgesia. Nature. 1983; 306:684–6. [PubMed: 6656868]

Foong FW, Duggan AW. Brain-stem areas tonically inhibiting dorsal horn neurones: studies with microinjection of the GABA analogue piperidine-4-sulphonic acid. Pain. 1986; 27:361–71. [PubMed: 3808742]

Foote SL, Aston-Jones G, Bloom FE. Impulse activity of locus coeruleus neurons in awake rats and monkeys is a function of sensory stimulation and arousal. Proc Natl Acad Sci USA. 1980; 77:3033–7. [PubMed: 6771765]

Frangos, Eleni, Ellrich, Jens, Komisaruk, Barry R. Non-invasive Access to the Vagus Nerve Central Projections via Electrical Stimulation of the External Ear: fMRI Evidence in Humans. Brain Stimulation. 2015; 8:624–36. [PubMed: 25573069]

Garcia R, Lin R, Lee J, Loggia M, Kim J, Kim H, Wasan A, Edwards R, Hadjikhani N, Napadow V. (395) Brainstem activity and connectivity is modulated by respiratory-gated auricular vagus afferent nerve stimulation (RAVANS) in migraine patients–an fMRI study. The Journal of Pain. 2016; 17:S73–S74.

Gebhart GF, Ossipov MH. Characterization of inhibition of the spinal nociceptive tail-flick reflex in the rat from the medullary lateral reticular nucleus. J Neurosci. 1986; 6:701–13. [PubMed: 2870140]

German DC, Walker BS, Manaye K, Smith WK, Woodward DJ, North AJ. The human locus coeruleus: computer reconstruction of cellular distribution. J Neurosci. 1988; 8:1776–88. [PubMed: 3367220]

Gizewski ER, Maderwald S, Linn J, Dassinger B, Bochmann K, Forsting M, Ladd ME. High-resolution anatomy of the human brain stem using 7-T MRI: improved detection of inner structures and nerves? Neuroradiology. 2014; 56:177–86. [PubMed: 24357075]

Glover GH, Li TQ, Ress D. Image-based method for retrospective correction of physiological motion effects in fMRI: RETROICOR. Magnetic Resonance in Medicine. 2000; 44:162–67. [PubMed: 10893535]

Goense J, Bohraus Y, Logothetis NK. fMRI at High Spatial Resolution: Implications for BOLD-Models. Front Comput Neurosci. 2016; 10:66. [PubMed: 27445782]

Grabner G, Poser BA, Fujimoto K, Polimeni JR, Wald LL, Trattnig S, Toni I, Barth M. A study-specific fMRI normalization approach that operates directly on high resolution functional EPI data at 7 Tesla. NeuroImage. 2014; 100:710–4. [PubMed: 24973602]

Graybiel AM, Aosaki T, Flaherty AW, Kimura M. The basal ganglia and adaptive motor control. Science (New York, NY). 1994; 265:1826–31.

Griswold MA, Jakob PM, Chen Q, Goldfarb JW, Manning WJ, Edelman RR, Sodickson DK. Resolution enhancement in single-shot imaging using simultaneous acquisition of spatial harmonics (SMASH). Magnetic Resonance in Medicine. 1999; 41:1236–45. [PubMed: 10371457]

Haacke EM, Tang J, Neelavalli J, Cheng YC. Susceptibility mapping as a means to visualize veins and quantify oxygen saturation. J Magn Reson Imaging. 2010; 32:663–76. [PubMed: 20815065]

Hahn A, Kranz GS, Seidel EM, Sladky R, Kraus C, Kublbock M, Pfabigan DM, Hummer A, Grahl A, Ganger S, Windischberger C, Lamm C, Lanzenberger R. Comparing neural response to painful electrical stimulation with functional MRI at 3 and 7 T. NeuroImage. 2013; 82:336–43. [PubMed: 23769917]

Hale MW, Lowry CA. Functional topography of midbrain and pontine serotonergic systems: implications for synaptic regulation of serotonergic circuits. Psychopharmacology (Berl). 2011; 213:243–64. [PubMed: 21088958]

Handwerker DA, Ollinger JM, D'Esposito M. Variation of BOLD hemodynamic responses across subjects and brain regions and their effects on statistical analyses. NeuroImage. 2004; 21:1639–51. [PubMed: 15050587]

Harriott AM, Schwedt TJ. Migraine is associated with altered processing of sensory stimuli. Curr Pain Headache Rep. 2014; 18:458. [PubMed: 25245197]

Haws CM, Williamson AM, Fields HL. Putative nociceptive modulatory neurons in the dorsolateral pontomesencephalic reticular formation. Brain Res. 1989; 483:272–82. [PubMed: 2706520]

Heckman CJ, Hyngstrom AS, Johnson MD. Active properties of motoneurone dendrites: diffuse descending neuromodulation, focused local inhibition. J Physiol. 2008; 586:1225–31. [PubMed: 17947305]

Heinricher, MM., Ingram, SL. 5.41 - The Brainstem and Nociceptive Modulation A2 - Masland, Richard H. In: Albright, Thomas D.Albright, Thomas D.Masland, Richard H.Dallos, PeterOertel, DonataFirestein, StuartBeauchamp, Gary K.Bushnell, M CatherineBasbaum, Allan I.Kaas, Jon H., Gardner, Esther P., editors. The Senses: A Comprehensive Reference. Academic Press; New York: 2008.

Hord ED, Evans MS, Mueed S, Adamolekun B, Naritoku DK. The effect of vagus nerve stimulation on migraines. The Journal of Pain: Official Journal of the American Pain Society. 2003; 4:530–4. [PubMed: 14636821]

Hornung JP. The human raphe nuclei and the serotonergic system. J Chem Neuroanat. 2003; 26:331–43. [PubMed: 14729135]

Hornykiewicz O, Kish SJ. Biochemical pathophysiology of Parkinson's disease. Adv Neurol. 1987; 45:19–34. [PubMed: 2881444]

Hosobuchi Y, Adams JE, Linchitz R. Pain relief by electrical stimulation of the central gray matter in humans and its reversal by naloxone. Science (New York, NY). 1977; 197:183–6.

Hughes AJ, Daniel SE, Kilford L, Lees AJ. Accuracy of clinical diagnosis of idiopathic Parkinson's disease: a clinico-pathological study of 100 cases. J Neurol Neurosurg Psychiatry. 1992; 55:181–4. [PubMed: 1564476]

Jezzard P, Balaban RS. Correction for geometric distortion in echo planar images from B0 field variations. Magnetic Resonance in Medicine. 1995; 34:65–73. [PubMed: 7674900]

Juchem C, Nixon TW, McIntyre S, Boer VO, Rothman DL, de Graaf RA. Dynamic multi-coil shimming of the human brain at 7 T. J Magn Reson. 2011; 212:280–8. [PubMed: 21824794]

Kalia M. Neuroanatomical organization of the respiratory centers. Fed Proc. 1977; 36:2405–11. [PubMed: 892012]

Karachi C, Grabli D, Bernard FA, Tande D, Wattiez N, Belaid H, Bardinet E, Prigent A, Nothacker HP, Hunot S, Hartmann A, Lehericy S, Hirsch EC, Francois C. Cholinergic mesencephalic neurons are involved in gait and postural disorders in Parkinson disease. J Clin Invest. 2010; 120:2745–54. [PubMed: 20628197]

Keltner JR, Furst A, Fan C, Redfern R, Inglis B, Fields HL. Isolating the modulatory effect of expectation on pain transmission: a functional magnetic resonance imaging study. J Neurosci. 2006; 26:4437–43. [PubMed: 16624963]

Keren NI, Lozar CT, Harris KC, Morgan PS, Eckert MA. In vivo mapping of the human locus coeruleus. NeuroImage. 2009; 47:1261–7. [PubMed: 19524044]

Keuken MC, Bazin PL, Crown L, Hootsmans J, Laufer A, Muller-Axt C, Sier R, van der Putten EJ, Schafer A, Turner R, Forstmann BU. Quantifying inter-individual anatomical variability in the subcortex using 7 T structural MRI. NeuroImage. 2014; 94:40–6. [PubMed: 24650599]

Kiyokawa J, Yamaguchi K, Okada R, Maehara T, Akita K. Origin, course and distribution of the nerves to the posterosuperior wall of the external acoustic meatus. Anat Sci Int. 2014; 89:238–45. [PubMed: 24604237]

Koob GF, Le Moal M. Drug addiction, dysregulation of reward, and allostasis. Neuropsychopharmacology: Official Publication of the American College of Neuropsychopharmacology. 2001; 24:97–129. [PubMed: 11120394]

Kraus T, Kiess O, Hosl K, Terekhin P, Kornhuber J, Forster C. CNS BOLD fMRI effects of sham-controlled transcutaneous electrical nerve stimulation in the left outer auditory canal - a pilot study. Brain Stimulation. 2013; 6:798–804. [PubMed: 23453934]

Kruger G, Glover GH. Physiological noise in oxygenation-sensitive magnetic resonance imaging. Magnetic Resonance in Medicine. 2001; 46:631–7. [PubMed: 11590638]

Kwon DH, Kim JM, Oh SH, Jeong HJ, Park SY, Oh ES, Chi JG, Kim YB, Jeon BS, Cho ZH. Seven-Tesla magnetic resonance images of the substantia nigra in Parkinson disease. Ann Neurol. 2012; 71:267–77. [PubMed: 22367998]

Lambert C, Lutti A, Helms G, Frackowiak R, Ashburner J. Multiparametric brainstem segmentation using a modified multivariate mixture of Gaussians. Neuroimage Clin. 2013; 2:684–94. [PubMed: 24179820]

Lang AE, Lozano AM. Parkinson's disease. First of two parts. N Engl J Med. 1998; 339:1044–53. [PubMed: 9761807]

Lau B, Welter ML, Belaid H, Vidal S Fernandez, Bardinet E, Grabli D, Karachi C. The integrative role of the pedunculopontine nucleus in human gait. Brain: A Journal of Neurology. 2015; 138:1284–96. [PubMed: 25765327]

Lavoie B, Smith Y, Parent A. Dopaminergic innervation of the basal ganglia in the squirrel monkey as revealed by tyrosine hydroxylase immunohistochemistry. J Comp Neurol. 1989; 289:36–52. [PubMed: 2572613]

Le Bars D. The whole body receptive field of dorsal horn multireceptive neurones. Brain Res Brain Res Rev. 2002; 40:29–44. [PubMed: 12589904]

Lee J, Lin RL, Garcia RG, Kim J, Kim H, Loggia ML, Mawla I, Wasan AD, Edwards RR, Rosen BR, Hadjikhani N, Napadow V. Reduced insula habituation associated with amplification of trigeminal brainstem input in migraine. Cephalalgia: An International Journal of Headache. 2016

Lehericy S, Bardinet E, Poupon C, Vidailhet M, Francois C. 7 Tesla magnetic resonance imaging: a closer look at substantia nigra anatomy in Parkinson's disease. Mov Disord. 2014; 29:1574–81. [PubMed: 25308960]

Leung LS, Luo T, Ma J, Herrick I. Brain areas that influence general anesthesia. Prog Neurobiol. 2014; 122:24–44. [PubMed: 25172271]

Li W, Wu B, Avram AV, Liu C. Magnetic susceptibility anisotropy of human brain in vivo and its molecular underpinnings. NeuroImage. 2012; 59:2088–97. [PubMed: 22036681]

Lima D, Almeida A. The medullary dorsal reticular nucleus as a pronociceptive centre of the pain control system. Prog Neurobiol. 2002; 66:81–108. [PubMed: 11900883]

Lindquist MA, Loh J Meng, Atlas LY, Wager TD. Modeling the hemodynamic response function in fMRI: efficiency, bias and mis-modeling. NeuroImage. 2009; 45:S187–98. [PubMed: 19084070]

Linnman C, Moulton EA, Barmettler G, Becerra L, Borsook D. Neuroimaging of the periaqueductal gray: state of the field. NeuroImage. 2012; 60:505–22. [PubMed: 22197740]

Luft AR, Skalej M, Schulz JB, Welte D, Kolb R, Burk K, Klockgether T, Voight K. Patterns of age-related shrinkage in cerebellum and brainstem observed in vivo using three-dimensional MRI volumetry. Cereb Cortex. 1999; 9:712–21. [PubMed: 10554994]

Luppi PH, Clement O, Sapin E, Peyron C, Gervasoni D, Leger L, Fort P. Brainstem mechanisms of paradoxical (REM) sleep generation. Pflugers Arch. 2012; 463:43–52. [PubMed: 22083642]

Macefield VG, Henderson LA. Real-time imaging of the medullary circuitry involved in the generation of spontaneous muscle sympathetic nerve activity in awake subjects. Human Brain Mapping. 2010; 31:539–49. [PubMed: 19777579]

Mai, JK., Assheuer, J., Paxinos, G. Atlas of the Human Brain. Elsevier Academic Press; San Diego: 2004.

Mainero C, Boshyan J, Hadjikhani N. Altered functional magnetic resonance imaging resting-state connectivity in periaqueductal gray networks in migraine. Ann Neurol. 2011; 70:838–45. [PubMed: 22162064]

Meara J, Bhowmick BK, Hobson P. Accuracy of diagnosis in patients with presumed Parkinson's disease. Age Ageing. 1999; 28:99–102. [PubMed: 10350403]

Meldrum BS. Glutamate as a neurotransmitter in the brain: review of physiology and pathology. J Nutr. 2000; 130:1007S–15S. [PubMed: 10736372]

Menke RA, Jbabdi S, Miller KL, Matthews PM, Zarei M. Connectivity-based segmentation of the substantia nigra in human and its implications in Parkinson's disease. NeuroImage. 2010; 52:1175–80. [PubMed: 20677376]

Mesulam MM, Mufson EJ, Levey AI, Wainer BH. Atlas of cholinergic neurons in the forebrain and upper brainstem of the macaque based on monoclonal choline acetyltransferase immunohistochemistry and acetylcholinesterase histochemistry. Neuroscience. 1984; 12:669–86. [PubMed: 6382047]

Moher Alsady T, Blessing EM, Beissner F. MICA-A toolbox for masked independent component analysis of fMRI data. Human Brain Mapping. 2016

Monti JM. The structure of the dorsal raphe nucleus and its relevance to the regulation of sleep and wakefulness. Sleep Med Rev. 2010; 14:307–17. [PubMed: 20153669]

Mori S, Oishi K, Faria AV. White matter atlases based on diffusion tensor imaging. Curr Opin Neurol. 2009; 22:362–9. [PubMed: 19571751]

Mori S, Oishi K, Jiang H, Jiang L, Li X, Akhter K, Hua K, Faria AV, Mahmood A, Woods R, Toga AW, Pike GB, Neto PR, Evans A, Zhang J, Huang H, Miller MI, van Zijl P, Mazziotta J. Stereotaxic white matter atlas based on diffusion tensor imaging in an ICBM template. NeuroImage. 2008; 40:570–82. [PubMed: 18255316]

Morris CM, Candy JM, Oakley AE, Bloxham CA, Edwardson JA. Histochemical distribution of non-haem iron in the human brain. Acta Anat (Basel). 1992; 144:235–57. [PubMed: 1529678]

Mosqueira AJ, Lopez-Manzanares L, Canneti B, Barroso A, Garcia-Navarrete E, Valdivia A, Vivancos J. Vagus nerve stimulation in patients with migraine. Revista De Neurologia. 2013; 57:57–63. [PubMed: 23836335]

Moss MS, Basbaum AI. The peptidergic organization of the cat periaqueductal gray. II. The distribution of immunoreactive substance P and vasoactive intestinal polypeptide. J Neurosci. 1983; 3:1437–49. [PubMed: 6191012]

Moss MS, Glazer EJ, Basbaum AI. The peptidergic organization of the cat periaqueductal gray. I. The distribution of immunoreactive enkephalin-containing neurons and terminals. J Neurosci. 1983; 3:603–16. [PubMed: 6827311]

Moulton EA, Burstein R, Tully S, Hargreaves R, Becerra L, Borsook D. Interictal dysfunction of a brainstem descending modulatory center in migraine patients. PloS One. 2008; 3:e3799. [PubMed: 19030105]

Moulton, Eric A., Becerra, Lino, Johnson, Adriana, Burstein, Rami, Borsook, David. Altered hypothalamic functional connectivity with autonomic circuits and the locus coeruleus in migraine. PloS One. 2014; 9:e95508. [PubMed: 24743801]

Naidich, Thomas P., Duvernoy, Henri M., Delman, Bradley N., Sorensen, A Gregory, Kollias, Spyros S., Haacke, E Mark. Duvernoy's Atlas of the Human Brain Stem and Cerebellum. Springer Vienna; Vienna: 2009.

Napadow, Vitaly, Dhond, Rupali, Conti, Giulia, Makris, Nikos, Brown, Emery N., Barbieri, Riccardo. Brain correlates of autonomic modulation: combining heart rate variability with fMRI. NeuroImage. 2008; 42:169–77. [PubMed: 18524629]

Napadow, Vitaly, Edwards, Robert R., Cahalan, Christine M., Mensing, George, Greenbaum, Seth, Valovska, Assia, Li, Ang, Kim, Jieun, Maeda, Yumi, Park, Kyungmo, Wasan, Ajay D. Evoked pain analgesia in chronic pelvic pain patients using respiratory-gated auricular vagal afferent nerve stimulation. Pain Medicine (Malden, Mass). 2012; 13:777–89.

Napadow, Vitaly, Lee, Jeungchan, Kim, Jieun, Cina, Stephen, Maeda, Yumi, Barbieri, Riccardo, Harris, Richard E., Kettner, Norman, Park, Kyungmo. Brain correlates of phasic autonomic response to acupuncture stimulation: an event-related fMRI study. Human Brain Mapping. 2013; 34:2592–606. [PubMed: 22504841]

Neff RA, Mihalevich M, Mendelowitz D. Stimulation of NTS activates NMDA and non-NMDA receptors in rat cardiac vagal neurons in the nucleus ambiguus. Brain Research. 1998; 792:277–82. [PubMed: 9593939]

Nomura S, Mizuno N. Central distribution of primary afferent fibers in the Arnold's nerve (the auricular branch of the vagus nerve): a transganglionic HRP study in the cat. Brain Research. 1984; 292:199–205. [PubMed: 6692153]

O'Herron P, Chhatbar PY, Levy M, Shen Z, Schramm AE, Lu Z, Kara P. Neural correlates of single-vessel haemodynamic responses *in vivo*. Nature. 2016; 534(7607):378–82. [PubMed: 27281215]

Parent, André. Carpenter's human neuroanatomy. Williams & Wilkins; 1996.

Parry DM, Macmillan FM, Koutsikou S, McMullan S, Lumb BM. Separation of A- versus C-nociceptive inputs into spinal-brainstem circuits. Neuroscience. 2008; 152:1076–85. [PubMed: 18328632]

Pattinson KT, Mitsis GD, Harvey AK, Jbabdi S, Dirckx S, Mayhew SD, Rogers R, Tracey I, Wise RG. Determination of the human brainstem respiratory control network and its cortical connections in vivo using functional and structural imaging. NeuroImage. 2009; 44:295–305. [PubMed: 18926913]

Paxinos, George, Huang, Xu-Feng. Atlas of the human brainstem. Elsevier; 2013.

Penny WD, Trujillo-Barreto NJ, Friston KJ. Bayesian fMRI time series analysis with spatial priors. NeuroImage. 2005; 24:350–62. [PubMed: 15627578]

Pertovaara A, Almeida A. Chapter 13 Descending inhibitory systems. Handb Clin Neurol. 2006; 81:179–92. [PubMed: 18808835]

Petroff OA. GABA and glutamate in the human brain. Neuroscientist. 2002; 8:562–73. [PubMed: 12467378]

Polimeni JR, Fischl B, Greve DN, Wald LL. Laminar analysis of 7T BOLD suing an imposed spatial activation pattern in human V1. Neuroimage. 2010; 52(4):1334–46. [PubMed: 20460157]

Poncelet BP, Wedeen VJ, Weisskoff RM, Cohen MS. Brain parenchyma motion: measurement with cine echo-planar MR imaging. Radiology. 1992; 185:645–51. [PubMed: 1438740]

Prats-Galino A, Soria G, de Notaris M, Puig J, Pedraza S. Functional anatomy of subcortical circuits issuing from or integrating at the human brainstem. Clinical Neurophysiology: Official Journal of the International Federation of Clinical Neurophysiology. 2012; 123:4–12. [PubMed: 22055838]

Raininko R, Autti T, Vanhanen SL, Ylikoski A, Erkinjuntti T, Santavuori P. The normal brain stem from infancy to old age. A morphometric MRI study. Neuroradiology. 1994; 36:364–8. [PubMed: 7936176]

Raj D, Paley DP, Anderson AW, Kennan RP, Gore JC. A model for susceptibility artefacts from respiration in functional echo-planar magnetic resonance imaging. Phys Med Biol. 2000; 45:3809–20. [PubMed: 11131201]

Reichenbach JR. The future of susceptibility contrast for assessment of anatomy and function. NeuroImage. 2012; 62:1311–5. [PubMed: 22245644]

Renvall V, Witzel T, Wald LL, Polimeni JR. Automatic cortical surface reconstruction of high-resolution T1 echo planar imaging data. NeuroImage. 2016; 134:338–54. [PubMed: 27079529]

Riederer P, Wuketich S. Time course of nigrostriatal degeneration in parkinson's disease. A detailed study of influential factors in human brain amine analysis. J Neural Transm. 1976; 38:277–301. [PubMed: 956814]

Salamone JD, Correa M. The mysterious motivational functions of mesolimbic dopamine. Neuron. 2012; 76:470–85. [PubMed: 23141060]

Sasaki M, Shibata E, Tohyama K, Takahashi J, Otsuka K, Tsuchiya K, Takahashi S, Ehara S, Terayama Y, Sakai A. Neuromelanin magnetic resonance imaging of locus ceruleus and substantia nigra in Parkinson's disease. Neuroreport. 2006; 17:1215–8. [PubMed: 16837857]

Satpute AB, Wager TD, Cohen-Adad J, Bianciardi M, Choi JK, Buhle JT, Wald LL, Barrett LF. Identification of discrete functional subregions of the human periaqueductal gray. Proc Natl Acad Sci USA. 2013; 110:17101–6. [PubMed: 24082116]

Schreihofer, Ann M., Guyenet, Patrice G. Baro-activated neurons with pulse-modulated activity in the rat caudal ventrolateral medulla express GAD67 mRNA. Journal of Neurophysiology. 2003; 89:1265–77. [PubMed: 12612005]

Schultz W. Updating dopamine reward signals. Curr Opin Neurobiol. 2013; 23:229–38. [PubMed: 23267662]

Sclocco R, Beissner F, Desbordes G, Polimeni JR, Wald LL, Kettner NW, Kim J, Garcia RG, Renvall V, Bianchi AM, Cerutti S, Napadow V, Barbieri R. Neuroimaging brainstem circuitry supporting cardiovagal response to pain: a combined heart rate variability/ultrahigh-field (7 T) functional magnetic resonance imaging study. Philos Trans A Math Phys Eng Sci. 2016; 374

Sclocco, Roberta, Kim, Jieun, Garcia, Ronald G., Sheehan, James D., Beissner, Florian, Bianchi, Anna M., Cerutti, Sergio, Kuo, Braden, Barbieri, Riccardo, Napadow, Vitaly. Brain Circuitry Supporting Multi-Organ Autonomic Outflow in Response to Nausea. Cerebral Cortex (New York, NY: 1991). 2014

Sharp T, Cowen PJ. 5-HT and depression: is the glass half-full? Curr Opin Pharmacol. 2011; 11:45–51. [PubMed: 21377932]

Sims-Williams H, Matthews JC, Talbot PS, Love-Jones S, Brooks JC, Patel NK, Pickering AE. Deep brain stimulation of the periaqueductal gray releases endogenous opioids in humans. NeuroImage. 2016

Son YD, Cho ZH, Choi EJ, Kim JH, Kim HK, Lee SY, Chi JG, Park CW, Kim JH, Kim YB. Individually differentiated serotonergic raphe nuclei measured with brain PET/MR imaging. Radiology. 2014; 272:541–8. [PubMed: 24654972]

Son YD, Cho ZH, Kim HK, Choi EJ, Lee SY, Chi JG, Park CW, Kim YB. Glucose metabolism of the midline nuclei raphe in the brainstem observed by PET-MRI fusion imaging. NeuroImage. 2012; 59:1094–7. [PubMed: 21963920]

Spyer KM. Neural organisation and control of the baroreceptor reflex. Reviews of Physiology, Biochemistry and Pharmacology. 1981; 88:24–124.

Stockmann JP, Witzel T, Keil B, Polimeni JR, Mareyam A, LaPierre C, Setsompop K, Wald LL. A 32-channel combined RF and B0 shim array for 3T brain imaging. Magnetic Resonance in Medicine. 2016; 75:441–51. [PubMed: 25689977]

Straube A, Ellrich J, Eren O, Blum B, Ruscheweyh R. Treatment of chronic migraine with transcutaneous stimulation of the auricular branch of the vagal nerve (auricular t-VNS): a randomized, monocentric clinical trial. The Journal of Headache and Pain. 2015; 16:543. [PubMed: 26156114]

Terman GW, Shavit Y, Lewis JW, Cannon JT, Liebeskind JC. Intrinsic mechanisms of pain inhibition: activation by stress. Science (New York, NY). 1984; 226:1270–7.

Terpstra M, Ugurbil K, Tkac I. Noninvasive quantification of human brain ascorbate concentration using 1H NMR spectroscopy at 7 T. NMR Biomed. 2010; 23:227–32. [PubMed: 19655342]

Thayer JF, Lane RD. A model of neurovisceral integration in emotion regulation and dysregulation. Journal of Affective Disorders. 2000; 61:201–16. [PubMed: 11163422]

Thevathasan W, Cole MH, Graepel CL, Hyam JA, Jenkinson N, Brittain JS, Coyne TJ, Silburn PA, Aziz TZ, Kerr G, Brown P. A spatiotemporal analysis of gait freezing and the impact of pedunculopontine nucleus stimulation. Brain: A Journal of Neurology. 2012; 135:1446–54. [PubMed: 22396391]

Tkac I, Gruetter R. Methodology of H NMR Spectroscopy of the Human Brain at Very High Magnetic Fields. Appl Magn Reson. 2005; 29:139–57. [PubMed: 20179773]

Tkac I, Oz G, Adriany G, Ugurbil K, Gruetter R. In vivo 1H NMR spectroscopy of the human brain at high magnetic fields: metabolite quantification at 4T vs. 7T. Magnetic Resonance in Medicine. 2009; 62:868–79. [PubMed: 19591201]

Tomasch J, Ebnessajjade D. The human nucleus ambiguus. A quantitative study. Anat Rec. 1961; 141:247–52. [PubMed: 13921693]

Tootell RB, Mendola JD, Hadjikhani NK, Ledden PJ, Liu AK, Reppas JB, Sereno MI, Dale AM. Functional analysis of V3A and related areas in human visual cortex. J Neurosci. 1997; 17:7060–78. [PubMed: 9278542]

Travagli RA, Hermann GE, Browning KN, Rogers RC. Brainstem circuits regulating gastric function. Annu Rev Physiol. 2006; 68:279–305. [PubMed: 16460274]

Triantafyllou C, Hoge RD, Krueger G, Wiggins CJ, Potthast A, Wiggins GC, Wald LL. Comparison of physiological noise at 1.5 T, 3 T and 7 T and optimization of fMRI acquisition parameters. NeuroImage. 2005; 26:243–50. [PubMed: 15862224]

Truong TK, Darnell D, Song AW. Integrated RF/shim coil array for parallel reception and localized B0 shimming in the human brain. NeuroImage. 2014; 103:235–40. [PubMed: 25270602]

Tzourio-Mazoyer N, Landeau B, Papathanassiou D, Crivello F, Etard O, Delcroix N, Mazoyer B, Joliot M. Automated anatomical labeling of activations in SPM using a macroscopic anatomical parcellation of the MNI MRI single-subject brain. NeuroImage. 2002; 15:273–89. [PubMed: 11771995]

Underwood MD, Khaibulina AA, Ellis SP, Moran A, Rice PM, Mann JJ, Arango V. Morphometry of the dorsal raphe nucleus serotonergic neurons in suicide victims. Biol Psychiatry. 1999; 46:473–83. [PubMed: 10459396]

van der Zwaag W, Schafer A, Marques JP, Turner R, Trampel R. Recent applications of UHF-MRI in the study of human brain function and structure: a review. NMR Biomed. 2015

van Gelderen P, de Zwart JA, Starewicz P, Hinks RS, Duyn JH. Real-time shimming to compensate for respiration-induced B0 fluctuations. Magnetic Resonance in Medicine. 2007; 57:362–8. [PubMed: 17260378]

van Laar PJ, Oterdoom DL Marinus, Ter Horst GJ, van Hulzen AL, de Graaf EK, Hoogduin H, Meiners LC, van Dijk JM. Surgical accuracy of 3-Tesla versus 7-Tesla MRI in Deep Brain Stimulation for Parkinson's Disease. World Neurosurg. 2016

Vazey EM, Aston-Jones G. Designer receptor manipulations reveal a role of the locus coeruleus noradrenergic system in isoflurane general anesthesia. Proc Natl Acad Sci USA. 2014; 111:3859–64. [PubMed: 24567395]

Ventureyra EC. Transcutaneous vagus nerve stimulation for partial onset seizure therapy. A new concept. Child's Nervous System: ChNS: Official Journal of the International Society for Pediatric Neurosurgery. 2000; 16:101–02.

Wargo CJ, Gore JC. Localized high-resolution DTI of the human midbrain using single-shot EPI, parallel imaging, and outer-volume suppression at 7T. Magn Reson Imaging. 2013; 31:810–9. [PubMed: 23541390]

Wehrwein, Erica A., Joyner, Michael J. Regulation of blood pressure by the arterial baroreflex and autonomic nervous system. Handbook of Clinical Neurology. 2013; 117:89–102. [PubMed: 24095118]

Windels F, Thevathasan W, Silburn P, Sah P. Where and what is the PPN and what is its role in locomotion? Brain: A Journal of Neurology. 2015; 138:1133–4. [PubMed: 25907754]

Wise RA. Drug-activation of brain reward pathways. Drug Alcohol Depend. 1998; 51:13–22. [PubMed: 9716927]

Worsley KJ, Friston KJ. Analysis of fMRI time-series revisited–again. NeuroImage. 1995; 2:173–81. [PubMed: 9343600]

Yezierski RP. Spinomesencephalic tract: projections from the lumbosacral spinal cord of the rat, cat, and monkey. J Comp Neurol. 1988; 267:131–46. [PubMed: 2449474]

Youssef AM, Gustin SM, Nash PG, Reeves JM, Petersen ET, Peck CC, Murray GM, Henderson LA. Differential brain activity in subjects with painful trigeminal neuropathy and painful temporomandibular disorder. Pain. 2014; 155:467–75. [PubMed: 24269492]

Yuan H, Silberstein SD. Vagus Nerve Stimulation and Headache. Headache. 2015

Zhuo M, Gebhart GF. Biphasic modulation of spinal nociceptive transmission from the medullary raphe nuclei in the rat. J Neurophysiol. 1997; 78:746–58. [PubMed: 9307109]

Zitella LM, Xiao Y, Teplitzky BA, Kastl DJ, Duchin Y, Baker KB, Vitek JL, Adriany G, Yacoub E, Harel N, Johnson MD. In Vivo 7T MRI of the Non-Human Primate Brainstem. PloS One. 2015; 10:e0127049. [PubMed: 25965401]

Zoccal DB, Furuya WI, Bassi M, Colombari DS, Colombari E. The nucleus of the solitary tract and the coordination of respiratory and sympathetic activities. Front Physiol. 2014; 5:238. [PubMed: 25009507]

Zrinzo L, Zrinzo LV, Tisch S, Limousin PD, Yousry TA, Afshar F, Hariz MI. Stereotactic localization of the human pedunculopontine nucleus: atlas-based coordinates and validation of a magnetic resonance imaging protocol for direct localization. Brain: A Journal of Neurology. 2008; 131:1588–98. [PubMed: 18467343]

Highlights

- The human brainstem plays a central role in the central nervous system, though it has been difficult to investigate due to physiological and anatomical characteristics.
- The broader adoption of ultrahigh-field (UHF) MRI scanning significantly advanced brainstem imaging.
- We discuss the advantages and the challenges of using UHF MRI for brainstem data acquisition and analysis.
- We illustrate how UHF MRI can shed new light on different brainstem-based circuitries, discuss existing and foreseeable clinical applications, and explore promising future directions.

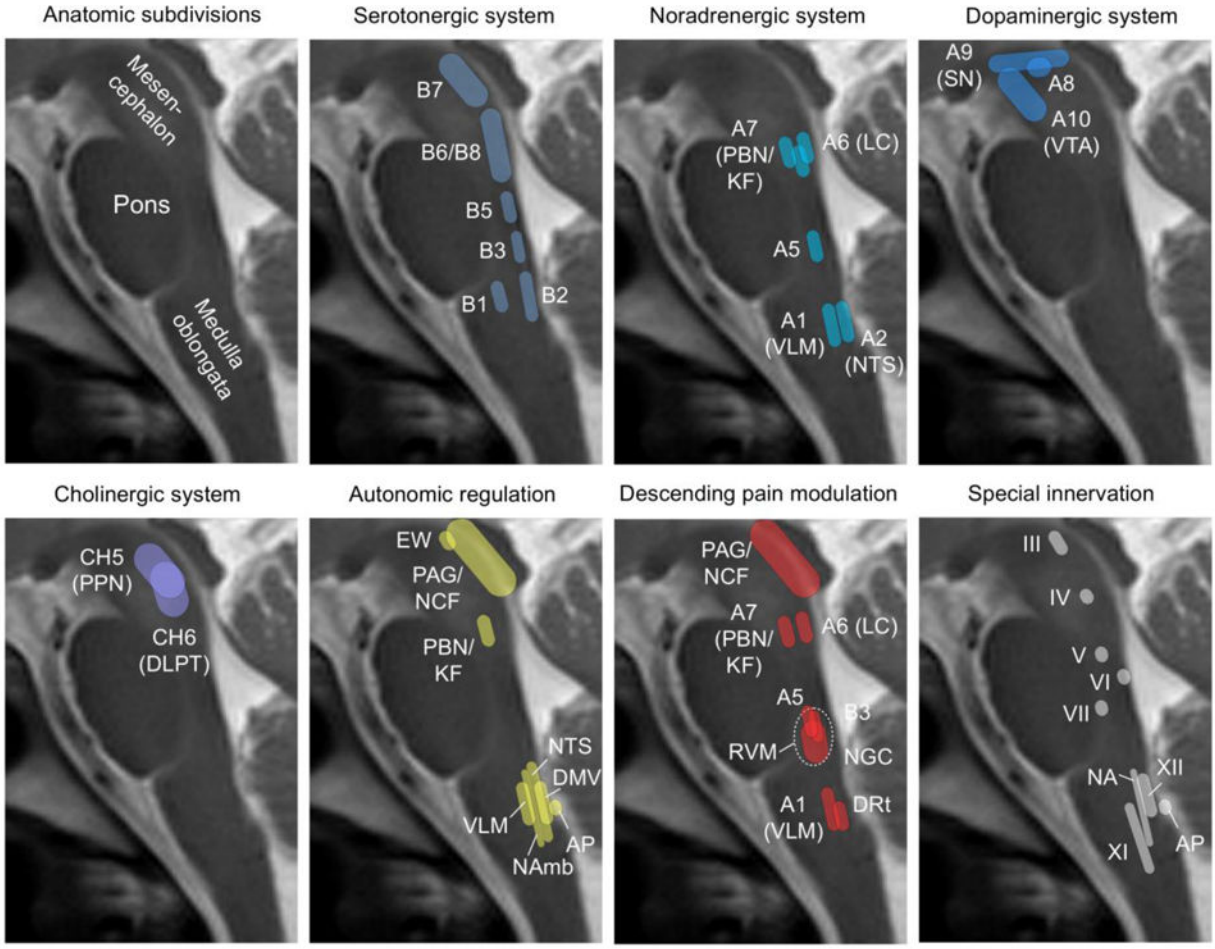

Figure 1.

Anatomical subdivisions and important functions of the brainstem. B1 to B8 denote the following serotonergic centers: Ncl. raphe pallidus (B1), Ncl. raphe obscurus (B2), Ncl. raphe magnus (B3), Ncl. raphe pontis (B5), Ncl. centralis superior (B6+B8), and Ncl. raphe dorsalis (B7). A1 to A7 denote nuclei of the noradrenergic system, and are located in the ventrolateral medulla (A1, VLM), the nucleus of the solitary tract (A2, NTS), near the superior olivary nucleus (A5), in the Locus coeruleus (A6, LC), and in the medial parabrachial and Kölliker-Fuse nuclei (A7, PBN/KF). The dopaminergic system in the midbrain consists of the centers A8 (unclear location), A9 (located in the in the substantia nigra, SN), and A10 (located in the ventral tegmental area, VTA). Cholinergic centers in the brainstem comprise the pedunculopontine reticular nucleus (CH5), and the dorsolateral pontine tegmentum (CH6). In addition to some of the previous nuclei, centers of autonomic control comprise Edinger-Westfal nucleus (EW), periaqueductal grey (PAG), Ncl. cuneiformis (NCF), Ncl. ambiguus (NAmb), Area postrema (AP), and Dorsal motor nucleus of the vagal nerve (DMV), whereas the descending pain modulatory system adds the Nct. reticularis gigantocellularis (NGC), which together with A5 forms the rostral ventromedial medulla (RVM), and the Dorsal reticular nucleus (DRt). Finally, there are nuclei with special motor functions including eye movement (Ncl. oculomotorius, III, Ncl. trochlearis, IV, and Ncl. abducens, VI), jaw movement (Ncl. motorius n. trigemini, V), facial expression (Ncl.

facialis, VII), tongue movement (Ncl. hypoglossus, XII), shoulder movement (Ncl. spinalis n. accessorii, XI), respiration (Ncl. ambiguus), and vomiting (Area postrema, AP).

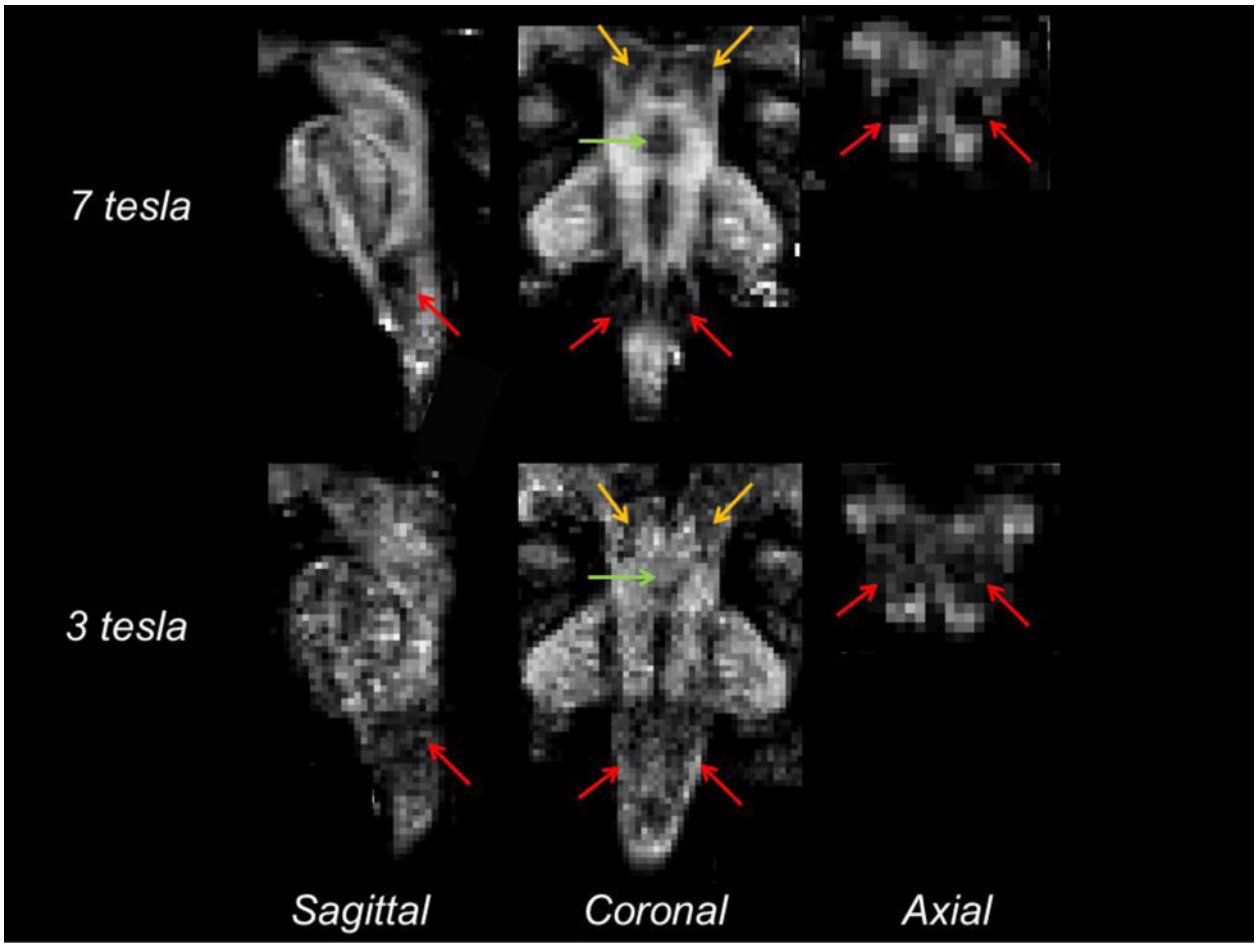

Figure 2. Sensitivity of structural MRI to visualize brainstem nuclei at 7 tesla and 3 tesla

We show for a healthy human subject the 1.1mm-isotropic-resolution diffusion fractional anisotropy map computed from diffusion tensor imaging acquired at 7 tesla (32 channel head coil, maximum achievable gradient amplitude = 70 mT/m) with echo time (TE) = 60.8 ms, TR = 5.6 s, total acquisition time about 25 minutes; and 3 tesla (32 channel head coil, maximum achievable gradient amplitude = 40 mT/m) with TE = 78.8 ms, TR = 8.5 s, total acquisition time about 37 minutes. Common 7 tesla and 3 tesla parameters were spin-echo EPI, b = 1000 s/mm^2, 60 directions/repetition, 7 “b0” (b = 0 s/mm^2) images/repetition, 4 repetitions. Note that the TE and TR were minimized in both scanners and that the same number of repetitions was employed. Our results suggest that an increased sensitivity and speed for brainstem nuclei delineation was achieved by using higher scanner magnetic field and gradient strength compared to conventional 3 tesla scanners. Arrows indicate inferior olivary nuclei (red), the median raphe (green), tegmental nuclei (yellow, such as the cuneiform nuclei).

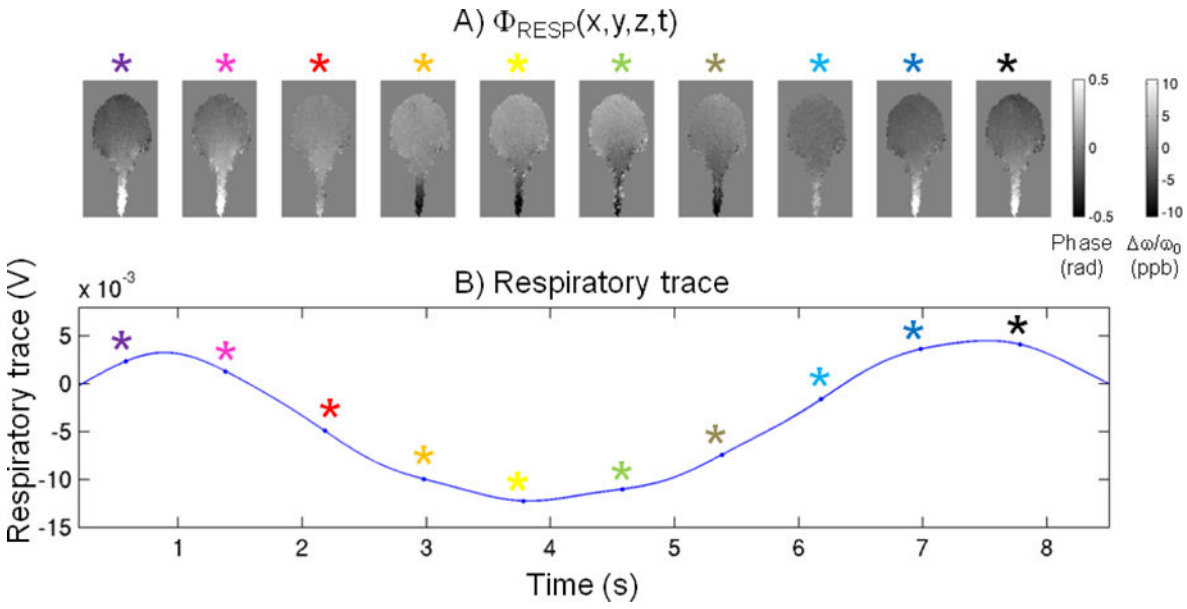

Figure 3. Chest motion effects are stronger in the brainstem and spinal cord than in brain regions more distal from the lungs

Upper row: phase changes (rad/ppb) in the brain due to respiration (one respiratory cycle shown) measured by phase gradient-echo EPI at 7 tesla (acquisition parameters: TR = 0.8 s; echo time = 25 ms; 160 repetitions, 2.5 × 2.5 × 2.5 mm^3, 15 coronal slices covering the brainstem, one slice shown; band-pass temporal filtering between 0.1 and 0.6 Hz applied to the phase EPI time-courses). Lower row: respiratory trace (downsampled at the MRI acquisition time, i.e. at each TR), recorded simultaneously with the phase MRI from a respiratory bellow positioned around the subject chest. Note that phase signal fluctuations induced by chest motion are about twice as high as in cortical areas.

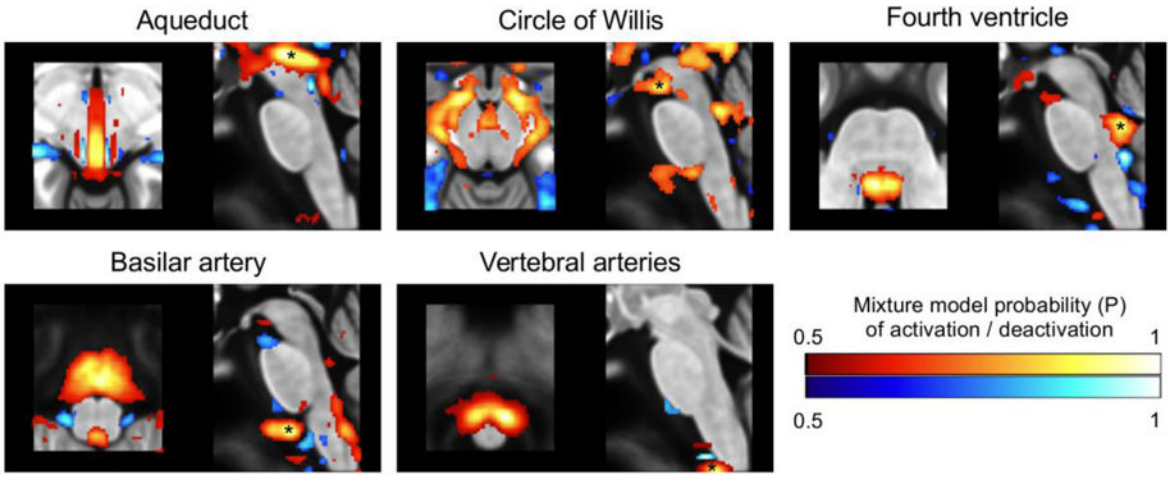

Figure 4. Regions of high signal variance in the brainstem as evidenced by independent component analysis (ICA) of brainstem-fMRI data

The figure shows selected components from a 16-dimensional ICA of the brainstem region (50 subjects, 10min resting-state fMRI, standard preprocessing). Results are clearly driven by physiological noise and reflect the strongest sources of pulsatile noise, namely the aqueduct, circle of Willis, fourth ventricle, as well as basilar and vertebral arteries (structures denoted with asterisks in the sagittal slices). The observation that these sources are mostly located outside the brainstem led to the development of masked ICA. Modified after (Beissner et al. 2014).

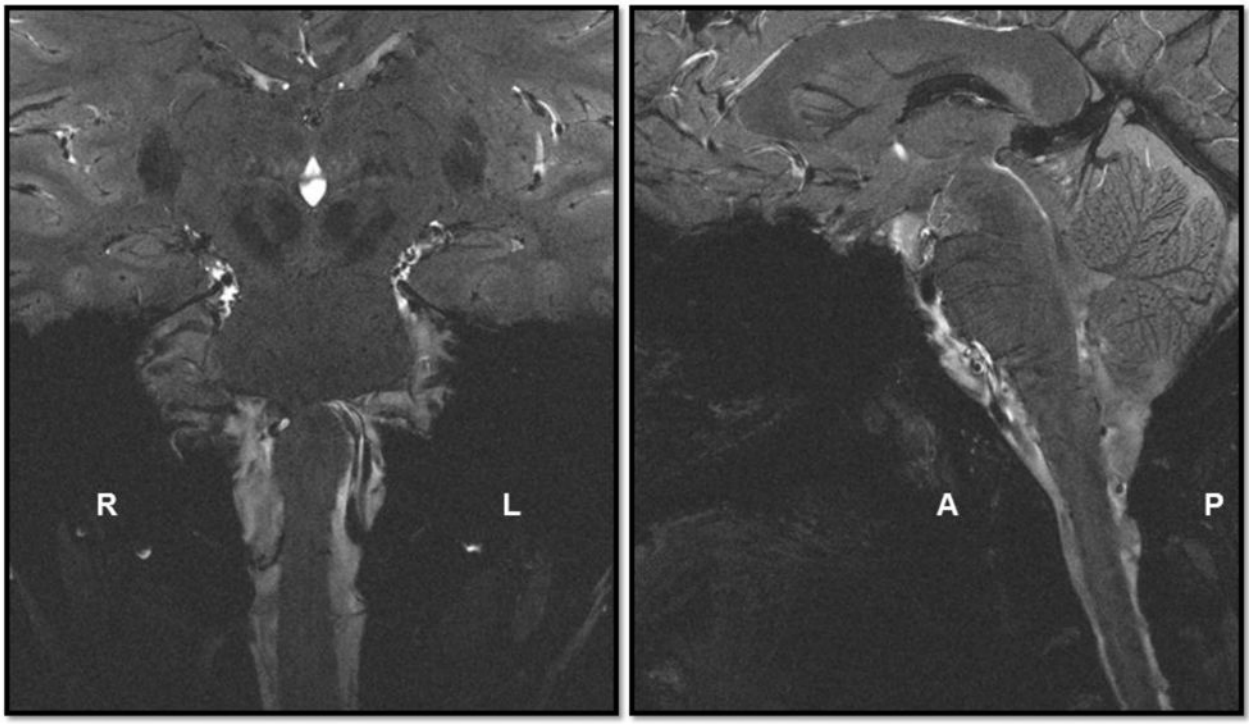

Figure 5.

Coronal (left) and sagittal (right) example frames from the movies depicting the brainstem during the cardiac cycle (links to the Supporting Movies S1 and S2 are available in the online version). The imaging data were retrospectively gated and the image was reconstructed at 25 evenly-spaced phases of the cardiac cycle.

Table 1

Anatomical characteristics of the brainstem nuclei described in the following sections. Reduced cross-sectional dimensions motivate the necessity for the increased spatial resolution afforded by UHF.

Nucleus	Brainstem anatomical subdivision	Primary neurotransmitter system(s)	Longitudinal dimension	Cross-sectional dimension	Reference
Raphe nuclei		Serotonergic			
Dorsal raphe nucleus (DR)	Midbrain		14.8 mm	20–25 mm^2	(Underwood et al. 1999; Bianciardi et al. 2015)
Median raphe nucleus (MnR)	Midbrain/Pons		10 mm (midline subgroup) 20 mm (paramedian subgroup)	5 mm^2 (midline subgroup) 10 mm^2 (paramedian subgroup)	(Baker et al. 1991)
Nucleus raphe magnus (RMg)	Pons/Medulla		10 mm	1.5 mm^2	(Hornung 2003; Bianciardi et al. 2015)
Locus Coeruleus (LC)	Pons	Noradrenergic	16 mm	1–2 mm^2	(German et al. 1988; Paxinos and Huang 2013)
Pedunculoponti ne nucleus (PPN)/peduncolotegmental nucleus (PTg)	Midbrain/Pons	Cholinergic	5 mm	6–8 mm^2	(Paxinos and Huang 2013; Zrinzo et al. 2008)
Substantia nigra (SN)	Midbrain	Dopaminergic	20 mm	10–15 mm^2	(Berg et al. 1999; Kwon et al. 2012)
Periaqueductal gray (PAG)	Midbrain	Dopaminergic, opioidergic	14 mm	4–5 mm radially on either side of the aqueduct	(Linnman et al. 2012)
Nucleus ambiguus (NAmb)	Medulla		10–11 mm	<1 mm^2	(Tomasch and Ebnessajja de 1961; Naidich et al. 2009)
Nucleus tractus solitarii (NTS)	Medulla		16 mm	<1 mm^2	(Büttner-Ennever and Horn 2013; Naidich et al. 2009)